Universitat Autònoma de Barcelona

A thesis for the

Master Telecommunications Engineering

Development of a batteryless RF receiver based on MEMS technology

by

Diego Alexis Chavez Montoya

Supervisor: Dr. Gabriel Abadal Berini

Department d'Enginyeria Electrònica

Escola d'Enginyeria (EE)

Universitat Autònoma de Barcelona (UAB)

Bellaterra, February 2020

El sotasignant, *Gabriel Abadal Berini*, professor de l'Escola d'Enginyeria (EE) de la Universitat Autònoma de Barcelona (UAB),

CERTIFICA:

Que el projecte presentat en aquesta memòria de Treball Final de Master ha estat realitzat sota la seva direcció per l'alumne *Diego Alexis Chavez Montoya*

I, perquè consti a tots els efectes, signa el present certificat.

Bellaterra, *5 de febrero de 2020*.

Signatura: *Gabriel Abadal Berini*

Resum

L'objectiu principal d'aquest projecte és desenvolupar un receptor sense fils i sense bateries basat en l'ús d'una estructura microelectromecànica com transductor d'energia electromagnètica; que és capaç de desmodular el senyal d'amplitud modulada rebut i produir un nivell de pressió de so audible. Al llarg del projecte, es van establir les bases teòriques relacionades amb el disseny d'antenes pegat i amb els sistemes microelectromecànics. A més, s'ha realitzat l'anàlisi, disseny i modelatge del receptor, tenint en compte diferents tipus d'estructures basades en tecnologia MEMS. Finalment, s'ha realitzat la mesura i anàlisi de resultats obtinguts al laboratori.

Resumen

El objetivo principal de este proyecto es desarrollar un receptor inalámbrico sin baterías basado en el uso de una estructura microelectromecánica como transductor de energía electromagnética; que es capaz de demodular la señal de amplitud modulada recibida y producir un nivel de presión de sonido audible. A lo largo del proyecto, se establecieron las bases teóricas relacionadas con el diseño de antenas parche y a los sistemas microelectromecánicos. Además, se ha realizado el análisis, diseño y con modelado del receptor; tomando en cuenta distintos tipos de estructuras basadas en tecnología MEMS. Por último, se ha realizado la medición y análisis de resultados obtenidos en laboratorio.

Summary

The main goal of this project is to develop a wireless receiver and batteryless based on the use of microelectromechanical structures as electromagnetic energy transducer, which is able to demodulate the amplitude modulated signal received and produce an audible sound pressure level. Along the project, it has been established the background related to microstrip antennas and microelectromechanical systems design. Besides, it has been done the analysis, design and modelling of the receiver, taking int account different types of structures based on MEMS technology. At the end, it has been done the measurements and analysis of the results obtained in the laboratory.

Contents

List of figures

List of Tables

1. Introduction

Nowadays, electronic and communication projects are focused to find solutions that help saving energy consumption. Most of them use batteries as their energy source but they have very limited lifetime. Additionally, other way to feed them based on the use of green energy (solar, wind, etc.) which represents a renewable source but it requires considerable area to work.

Along the years, many of the studies related to the reuse of Radio Frequency energy were linked to energy harvesting as a possible way to save energy. Probably, one of the most challenging goal to develop electronic circuits is to find the way to feed devices.

The study performed in this project is focused on using an AM modulated Radio Frequency signal to transmit information between wireless communication link and, at the same time, transmit the energy needed by the receiver to operate the transmitter and the receiver, so, through the excitation of a microelectromechanical element, it allows us to obtain a similar response as an electronic receiver. Due to the non-linear characteristic response of MEMS, it is possible to implement some of them to the stages of a direct amplitude modulated receiver, as well as the final electromechanical transducer that converts the demodulated signal in a sound pressure level.

To understand how the proposed device works, it has been studied the physics related to the functioning of microelectromechanical elements which are described in the next chapters.

1.1. Background

Many of the scientific articles related to the application of microelectromechanical technologies as a renewable source of energy are focused on the fabrication of sensors, actuators and energy harvesting.

The article [1] shows that it is possible to apply MEMS to reuse energy which comes from RF (radio frequency) sources. Although, the power received is extremely low, it could be used to feed some load. Other article like [2] shows a possible approach for RF energy harvesting and management based on the Improved Energy Efficient Ant Based Routing Algorithm.

Probably, the most closely related article to the current project is [3], which explains about the use of RF to feed a low power wake-up receiver application. This type of devices

involved in IoT needs a different way of power source because the use of batteries is impractical in large number of scenarios. They demonstrated that a way to achieve this goal is to dedicate an extremely low power receiver to wake up the system's power-hungry radio only when a particular trigger signal is present.

1.2. Statement of the problem

The problem refers to the reuse of the energy delivered by a fixed transmitter which operates at a given frequency, for transmitting an amplitude modulated signal to an audio receiver that could reproduce it in its speaker. As it has been mentioned in the introduction and background, the use of microelectromechanical systems MEMS could help to achieve this goal.

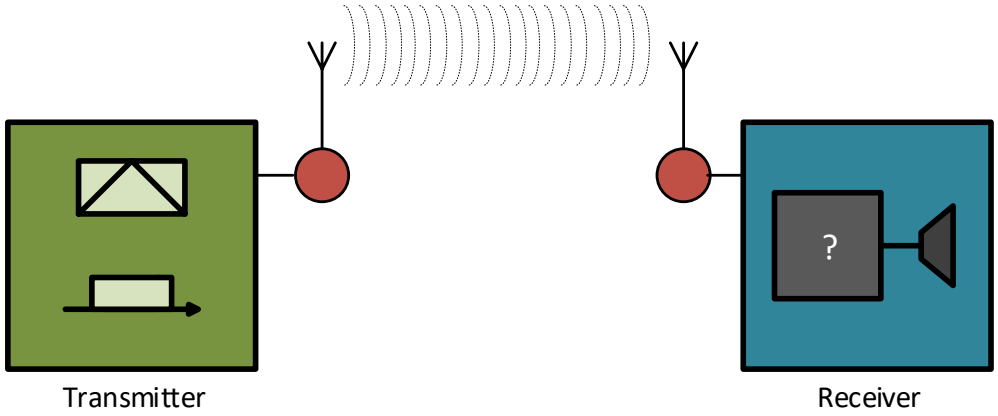

Figure 1: Basic system diagram

Therefore, the problem to solve is

How to move a mechanical structure based on converting the electromagnetic energy to mechanical energy. Finally, reusing RF energy for transmitting audio to a receiver without the use of batteries or other power sources.

1.3. Purpose of the study

The purpose of this project is to demonstrate that Microelectromechanical Systems (MEMS) could be the basis of a novel solution to receivers, which use non-conventional strategies not only to power supply but also to reproduce the information received. In figure 1, it is possible to show a block in question mark which represents the block in charge of filtering and demodulating the signal received. In figure 2, the question mark block is replaced by a block which shows a clamped free beam "Cantilever" as the element that can emulate the filter and the demodulation stages.

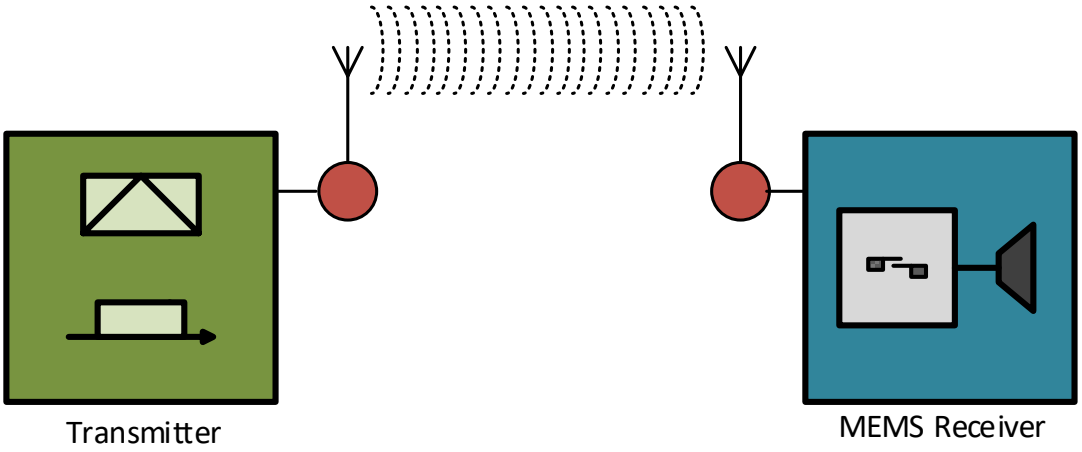

Figure 2:Basic system diagram using MEMS

1.4. Research Goals

The main goal of this project is to

Develop a batteryless receiver based on MEMS technology.

Therefore, MEMS theory requires the establishment of some steps which allow us to obtain a similar response compare to a conventional receiver. The steps to be developed are

- To analyze the stages involved in the receiver
- To design the communication link between the transmitter and the receiver
- To model the structure of the system

1.5. Structure

This project contains five chapters sequentially organized accordingly to the development process.

The Chapter 1 shows the introduction, the goals, the problem statement and previous background that have been studied along the years from different points of view.

In Chapter 2 shows some theoretical concepts about antennas design, receivers, and microelectromechanical systems which are the basis of this project. The receiver section describes the stages involved into signal processing identifying the differences between the types of receivers. The antenna's section describes the methodology of microstrip antennas design focused in rectangular patches. In Microelectromechanical section two types of structures which are commonly used like parallel and comb-drive beams were

described. Furthermore, the characteristic equations have been developed and described too.

Chapter 3 is focused on the analysis, design and modelling of the proposed system. It shows the results obtained in simulation stage where some applications like Feko software as antenna simulator and Matlab to model mathematically the system were used.

Chapter 4 shows the results and the analysis of data obtained in the laboratory. The measurements and calculus of values like the sound pressure level are shown.

In Chapter 5, the conclusions of each stage along the project are described.

2. Theory

2.1. Radio Frequency Receiver

The term Radio frequency RF is related to the oscillation rate in an electromagnetic field or in a mechanical system. Commonly, the radio frequency range goes from 20 KHz to 300 GHz. According to the radio spectrum designated by the International Telecommunications Union, these frequencies goes from Low Frequency to Extremely High Frequency.

The goal of a RF receiver is to process the incoming signal into usable form, adding minimum of distortion. [4] Consequently, a typical receiver includes the following sections

- The radio frequency section is in charge to select and to amplify the incoming signal in order to feed the demodulator section.
- The demodulator section demodulates the input signal and extract from it, the signal which was previously modulated in the transmitter.
- The post-demodulation section amplifies the demodulated signal up to the required level to operate output devices such as loudspeakers, earphones and/or TV screens.

It is normally taken as the minimum input signal required to produce a specified output signal having a specified signal to noise ratio as

$$S_{min} = \left(\frac{S}{N}\right)_{min} \cdot k \cdot T_0 \cdot B \cdot (NF) \tag{2.1}$$

Where $\left(\frac{S}{N}\right)_{min}$ is the minimum signal to noise ratio needed to process a signal, NF is the Noise figure factor, k is the Boltzmann's constant ($1.38x10^{-23}\ J/°K$), T_0 is the absolute temperature of the receiver input ($290\ °K$) and B is the bandwidth in Hz.

The signal to noise ratio in a receiver is the signal power in the receiver divided by the mean power of the receiver. The acceptable $\left(\frac{S}{N}\right)_{min}$ for a receiver depends on the intended use of the receiver.

It is a measure of the ability of a radio receiver to select the desired transmitted signal and to reject other signals nearby in frequency [5]. The selectivity performance determines the level of interference.

2.2. Amplitude modulation principles

Amplitude modulation is the process of varying the amplitude of the sinusoidal carrier wave by the amplitude of the modulating signal. As a consequence, the message signal becomes the modulating signal and it is transmitted by variations in the amplitude of the carrier. [6]

Basically, the frequency carrier works in higher frequency than the modulating signal because it has the ability to travel over long distance comparing to the modulating signals and it can be used to transmit the information through space as an electromagnetic wave. The carrier frequencies are divided in the following domains

- Ultrahigh frequencies ranging from 300 MHz to 3 GHz, which gives a typical wavelength ranging from 1 meter to 10 centimeters.
- Superhigh frequencies ranging from 3 to 30 GHz which is ranging from 10 to 1 centimeter wavelength.
- Extremely high frequencies ranging from 30 to 300 GHz with a wavelength ranging from 1 centimeter to 1 millimeter.

Probably, the most used application in communication projects is the transmission of the audio signals to the conventional receivers like telephones, radio receivers, etc. They received and process the incoming signal to an audible frequency. The audible frequency is a periodic vibration whose frequency is in the band audible to the average human. Generally, the accepted hearing range for humans is ranging from 20 to 20 KHz. So, in air at atmospheric pressure where the air velocity is set to $c_{air} = 343\, m/s$, these represent sound waves with wavelengths from 17 meters to 17 meters to 1.7 centimeters. It is important to mention that frequencies below 20 Hz generally felt rather than heard and higher frequencies are the first to be affected by hearing loss due to age or prolonged exposure.

The fundamental frequency in audio applications is given by the pitch. It is an auditory sensation in which a listener assigns musical tones to relative positions on a musical scale based primarily on their perception of the frequency of vibration. Therefore, the voice speech of an adult male has a fundamental frequency from 85 to 180 Hz, and for adult female varies from 165 to 255 Hz. In telephony, the usable voice frequency band ranges from 300 to 3.4 KHz. It is for this reason that the ultra-low frequency band of the electromagnetic spectrum between 300 and 3000 Hz is also referred to as voice

frequency, being the electromagnetic energy that represents acoustic energy at baseband. The bandwidth related to voice frequency transmission channel is usually 4 KHz.

2.2.1. Equation of Amplitude Modulation

In amplitude modulation, the amplitude of the carrier signal is varied according to variations in the amplitude of the signal. The Figure 3 shows the modulating signal which is defined as $e_m = A \cdot \sin(2 \cdot \pi \cdot f_m \cdot t)$. Where the amplitude is set to 1 volt and the frequency is set to 100 Hz as an example. [7]

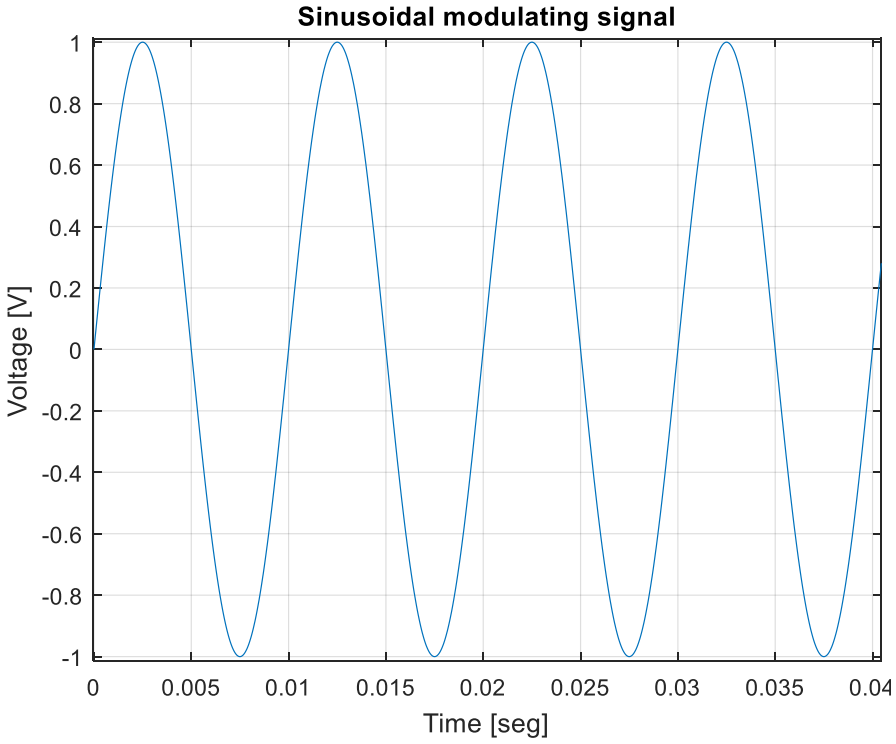

Figure 3:Sinusoidal modulating signal

The Figure 4 shows the sinusoidal high frequency carrier that is used to carry the message required. It is given as $e_c = A \cdot \sin(2 \cdot \pi \cdot f_c \cdot t)$. Where the amplitude is set to 1 volt and the frequency is set to 1 GHz as an example.

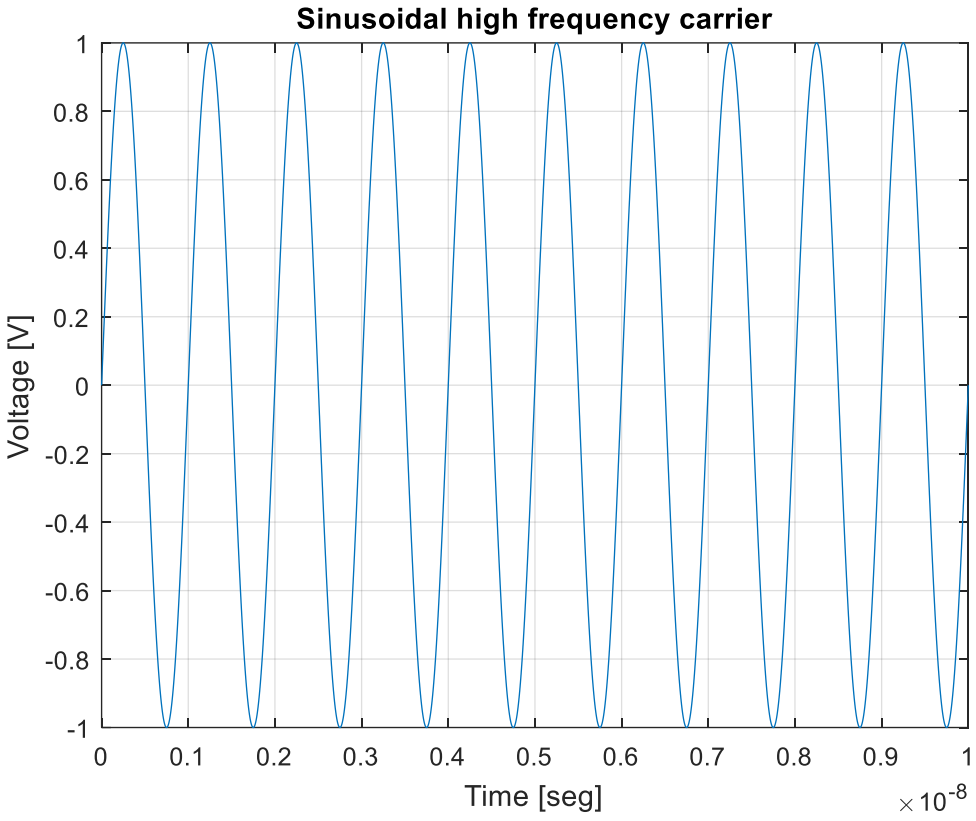

Figure 4: Sinusoidal high frequency carrier

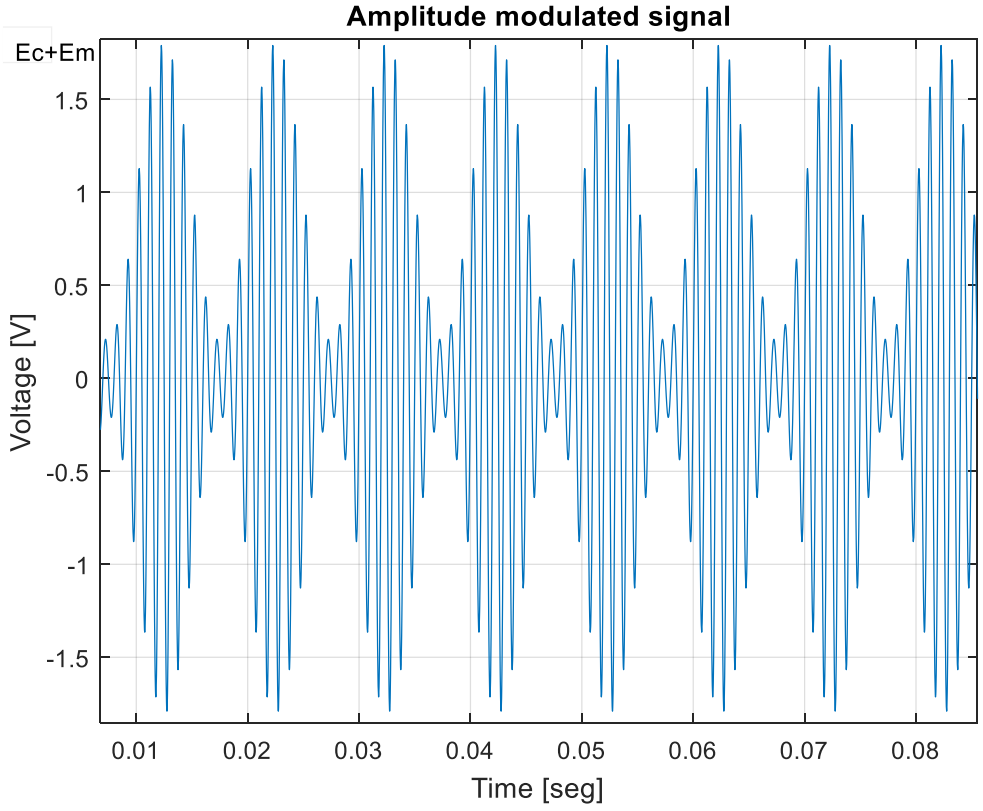

Figure 5:Amplitude modulated signal

As a result, in figure 5 the amplitude modulated signal is obtained. It is observed that the carrier frequency remains the same, but its amplitude varies according to amplitude variations of the modulating signal.

In general, the modulating signal equation is given as,

$$e_m = E_m \sin w_m t \tag{2.2}$$

And carrier signal can be represented by e_c as,

$$e_c = E_c \sin w_c t \tag{2.3}$$

The mathematical expressions described for modulating and carrier signals, we can create the mathematical expression of the complete modulated wave. It is given as,

$$E_{AM} = E_c + e_m \tag{2.4}$$

$$E_{AM} = E_c + E_m \sin w_m t \tag{2.5}$$

The instantaneous value of the amplitude modulated wave can be given as,

$$e_{AM} = (E_c + E_m \sin w_m t) \sin w_c t \tag{2.6}$$

2.2.2. Modulation index

The ratio of maximum amplitude of modulating signal to maximum amplitude of carrier signal is called modulation index, [6]

$$m = \frac{E_m}{E_c} \tag{2.7}$$

The value of the amplitude of the modulating signal E_m must be less than the amplitude of the carrier signal E_c to avoid any distortion in the modulated signal. Hence maximum value of modulation index will be equal to 1 when $E_m = E_c$.

If modulation index is higher than 1, the overmodulation signal appears and data is lost in such case. When modulation index is expressed in percentage, it is also called percentage modulation.

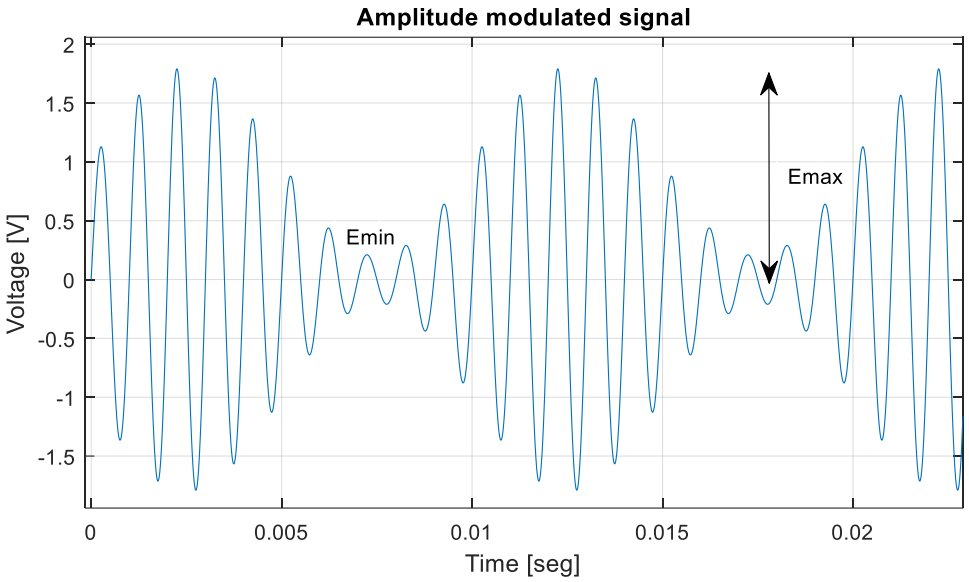

Figure 6: Amplitude modulated signal rides

It is clear from figure 6 that the modulating signal rides upon the carrier signal as

$$E_m = \frac{E_{max} - E_{min}}{2} \tag{2.8}$$

$$E_c = \frac{E_{max} + E_{min}}{2} \tag{2.9}$$

Taking the ratio of both equations, we can determine the index of modulation graphically as

$$m = \frac{E_{max} - E_{min}}{E_{max} + E_{min}} \tag{2.10}$$

2.2.3. Frequency spectrum and bandwidth

The modulated carrier has new signals at different frequencies, called side frequencies or sidebands. They occur above and below the carrier frequency

$$f_{USB} = f_c + f_m \tag{2.11}$$

$$f_{LSB} = f_c - f_m \tag{2.12}$$

Here f_c is carrier frequency, f_m is modulating signal frequency, f_{LSB} is lower sideband frequency and f_{USB} is upper sideband frequency.

Consider the expression of AM wave given by

$$e_{AM} = (E_c + E_m \sin w_m t) \sin w_c t \tag{2.13}$$

We know that $m = E_m/E_c$ and putting this value of E_m in above equation we get

$$e_{AM} = E_c \sin w_c t + mE_m \sin w_m t \sin w_c t \tag{2.14}$$

We know that $\sin(A)\sin(B) = \frac{1}{2}\cos(A-B) - \frac{1}{2}\cos(A+B)$. Applying this result to las term above equation we get

$$e_{AM} = E_c \sin w_C t + \frac{mE_c}{2}\cos(w_c - w_m)t - \frac{mE_c}{2}\cos(w_c + w_m)t \tag{2.15}$$

In the equation above, the first term represents unmodulated carrier, the second term represents lower sideband and last term represents upper sideband. Note that $w_c = 2\pi f_c$ and $w_m = 2\pi f_m$. Hence above equation can also be written as,

$$e_{AM} = E_c \sin 2\pi f_c t + \frac{mE_c}{2}\cos(2\pi f_{USB})t - \frac{mE_c}{2}\cos(2\pi f_{LSB})t \tag{2.16}$$

From this equation we can prepare the frequency spectrum of AM wave as shown below

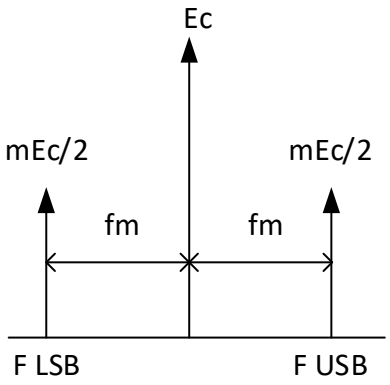

Figure 7: Frequency domain representation of AM wave

This contains full carrier and both the sidebands; hence it is also called Double Sideband Full Carrier system. Once, we know that bandwidth of the signal can be obtained by taking the difference between highest and lowest frequencies. From figure 7 we can obtain bandwidth of AM wave as,

$$BW = f_{USB} - f_{LSB} = 2f_m \tag{2.17}$$

Thus, bandwidth of AM signal is twice of the maximum frequency of modulating signal.

2.2.4. AM Power Distribution

We know that AM signal has three components: unmodulated carrier, lower sideband and upper sideband. Hence total power of AM wave is the sum of carrier power P_c and powers in the two sidebands P_{USB} and P_{LSB}

$$P_{Total} = P_c + P_{USB} + P_{LSB} = \frac{E_c^2}{R} + \frac{E_{LSB}^2}{R} + \frac{E_{USB}^2}{R} \quad (2.18)$$

Here all the three voltages are rms values and R is characteristic impedance of antenna in which the power is dissipated. The carrier power is

$$P_c = \frac{E_c^2}{2R} \quad (2.19)$$

The power of upper and lower sidebands is

$$P_{LSB} = P_{USB} = \frac{E_{SB}^2}{2R} \quad (2.20)$$

We know that the peak amplitude of both the sidebands is $\frac{mE_c}{2}$. Hence

$$E_{SB} = \frac{mE_c}{2\sqrt{2}} \quad (2.21)$$

$$P_{LSB} = P_{USB} = \frac{m^2E_c^2}{8R} \quad (2.22)$$

Hence the total power becomes,

$$P_{total} = \frac{E_c^2}{2R} + \frac{m^2E_c^2}{8R} + \frac{m^2E_c^2}{8R} = \frac{E_c^2}{2R}(1 + \frac{m^2}{2}) \quad (2.23)$$

$$P_{total} = P_c(1 + \frac{m^2}{2}) \quad (2.24)$$

$$\frac{P_{total}}{P_c} = 1 + \frac{m^2}{2} \quad (2.25)$$

This equation relates total power of AM wave to carrier power. Maximum value of modulation index, $m = 1$ to avoid distortion. So, at the maximum modulation index,

$$P_{total} = 1.5P_c \quad (2.26)$$

From above equations we have

$$m = \sqrt{2(\frac{P_{total}}{P_c} - 1)} \quad (2.27)$$

2.2.5. AM Receivers

Basically, the receivers can be grouped as:

a) **Tuned Radio Frequency Receiver**: It consists of two stages of tuned amplifiers, detector and audio amplifiers. The RF amplifier is simply tuned to the required signal then filter and amplify the received AM signal and pass it to detector stage.

The detector obtains the modulating audio signal to high power levels and drive the speaker.

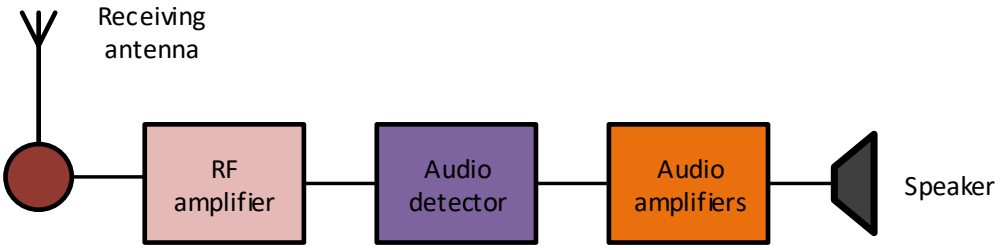

Figure 8: Tuned Radio Frequency Receiver stages

b) **The super heterodyne receiver** converts all incoming RF frequencies to fixed lower frequency, called Intermediate Frequency (IF). This IF is then amplified and detected to get the original signal.

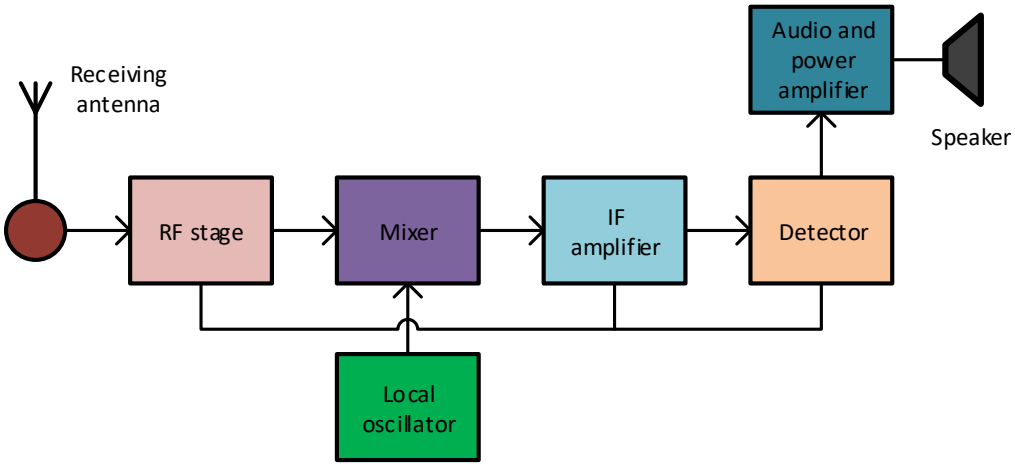

Figure 9: Super heterodyne Receiver stages

RF stage, the antenna receives all the frequency signals and gives it to RF amplifier. The RF stage amplifies the signals in the required range of frequencies. Thus, it provides initial gain and selectivity.

Mixer and Local Oscillator, the output of the RF amplifier is given to the mixer stage. The local oscillator output is also applied to the mixer.

IF Amplifier, the IF is amplified by one or more IF amplifier stages and given to the detector. Most of the gain and selectivity is provided by these IF amplifiers. Normally IF is fixed for the AM receivers. To select a particular station, the local oscillator frequency is changed in such a way that the frequency f_s of the station and f_0 has the difference equal to IF.

Automatic Gain Control, a part of output is taken from the detector and it is applied the RF amplifier, mixer and IF amplifiers for gain control.

Detector, the detector converts AM signal at IF to original modulating signal.

Audio and power amplifier, the signal received from detector is very weak and hence needs amplification audio power amplifiers normally have one or more stages. This signal is amplified and given to speaker.

c) **Direct-conversion receiver**, a new kind of super heterodyne receiver was introduced: the direct-conversion receiver (DCR) type, also known as the zero IF receiver. At first, the direct-conversion receiver seems attractive from an implementation point of view because of its simplicity.

With the rapid development of wireless communications, direct-conversion transceivers on a chip have experienced a huge evolution. A very high degree of integration is now possible allowing for the use of low-voltage, low-power circuits with built-in image cancellation circuits right on the chip. These new designs have been used in many modern wireless transceivers, communications receivers, and radar. Although the simplicity of a direct-conversion receiver is very attractive, rejecting the image content in this type of super heterodyne became the main challenge for designers of direct conversion architecture. [6]

2.3. Microstrip patch antenna

The expression 'patch' is derived from the shape of the printed conductor of the antenna: traditionally rectangular or circular.

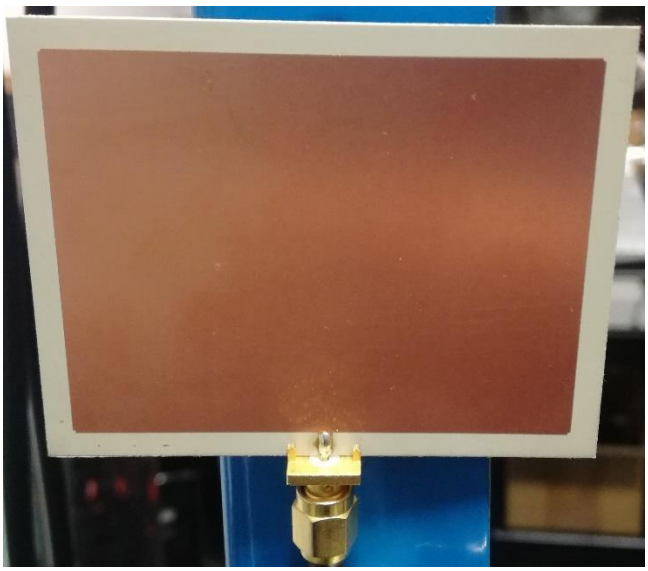

Figure 10: Rectangular patch microstrip antenna photo

Microstrip patch antennas are typically resonant in style as opposed to traveling wave and therefore are characterized by being quite efficient over a relatively narrow operation

bandwidth. A microstrip patch antenna is a resonant-style radiator so one of its dimensions must be approximately $\lambda_g/2$ where λ_g is a guided wavelength taking into consideration the surrounding environment of the printed antenna. The resonant dimension depends on the shape of the patch conductor. Having said this it will be become apparent that the properties of the substrate, namely its dielectric constant, ε_r and its height will play a fundamental role in the performance of the printed antenna.

Practically, when a voltage is applied to the feeding point the radiator, a current will be excited on the patch and vertical electric fields will be generated between the patch and the ground plane. The radiation efficiency will depend upon the material used, as the confinement of the fields will be determined by the dielectric constant of the substrate and its height.

2.3.1. Excitation methods of microstrip patches

The way a microstrip patch antenna is excited will determine the achievable impedance bandwidth (indirectly), the purity and direction of the radiated fields, the efficiency of the overall antenna, the ease of manufacturing of the antenna and its robustness. There are four fundamental techniques to feed or excite a microstrip patch antenna.

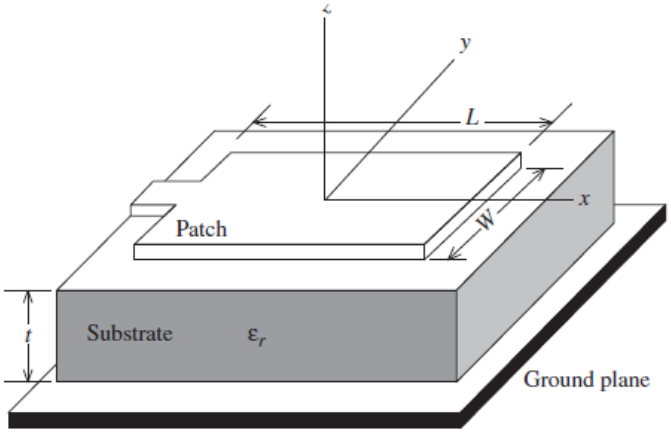

Figure 11: Geometry for analyzing the edge-fed microstrip patch antenna [8].

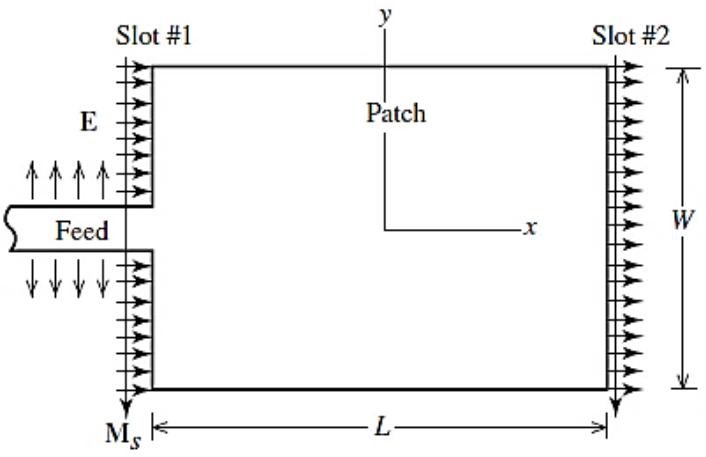

Figure 12: Rectangular microstrip patch antenna with equivalent horizontal radiating slots [8]

- Edge fed patches: A microstrip feed-line of width w_f is in direct contact with a rectangular patch conductor of length L and width W. The patch resides on a grounded substrate of thickness, d and dielectric constant, ε_r.

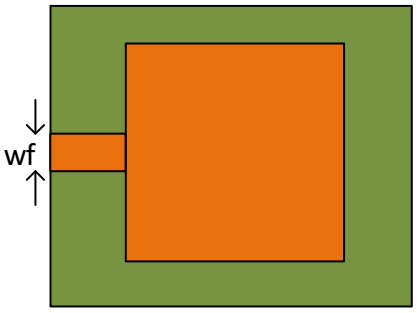

Figure 13: Edge fed patch in rectangular microstrip antenna

- Probe fed patches: The probe or feeding pin is usually the inner conductor of a coaxial line; hence probe-feeding is often referred to as a coaxial feed. The probe position provides the impedance control in a similar manner to inserting the feed for an edge-fed patch. Because of the direct contact between the feed transmission line and the patch antenna, probe feeding is referred to as a direct contact excitation mechanism.

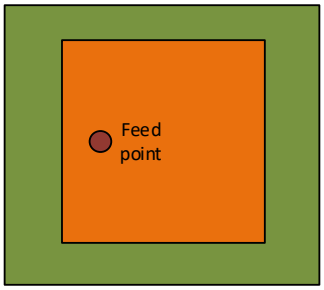

Figure 14: Probe fed patch in rectangular microstrip antenna

- Proximity coupled patches: The microstrip antenna consists of a grounded substrate where a microstrip feedline terminated with an open circuit is located. Above this material is another dielectric laminate with a microstrip patch etched on its top surface.

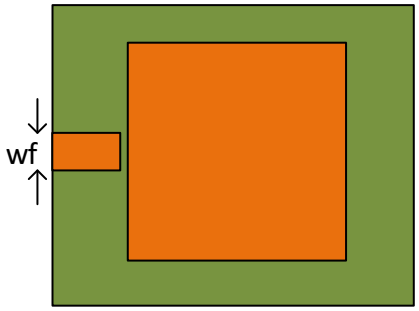

Figure 15: Proximity coupled patch in rectangular microstrip antenna

- Aperture coupled patches: A separate laminates are used for the feed network and the patch antenna. The laminates are separated by a ground plane and coupling between the feed, in this case a microstrip line, and the patch antenna is achieved via a small slot in the ground plane. [9]

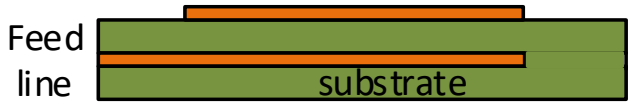

Figure 16: Aperture coupled patch in rectangular microstrip antenna

2.3.2. Methods of analysis

The microstrip antennas generally has a two-dimensional radiating patch on a thin dielectric substrate and therefore may be categorized as a two-dimensional planar component for analysis purposes. The analysis methods for MSAs can be broadly divided into two groups. [9]

In the first group, the methods are based on equivalent magnetic current distribution around the patch edges (similar to slot antennas).

- The transmission line model refers to the microstrip radiator element is viewed as a transmission line resonator with no transverse field variations, and the radiation occurs mainly from the fringing fields at the open circuited ends.
- The cavity model, the region between the patch and the ground plane is treated as a cavity that is surrounded by magnetic walls around the periphery and by electric walls from the top and bottom sides.

- The Multiport network model, is an extension of the cavity model. In this method, the electromagnetic fields underneath the patch and outside the patch are modeled separately. The patch is analyzed as a two-dimensional planar network, with a multiple number of ports located around the periphery.

In the second group, the methods are based on the electric current distribution on the patch conductor and the ground plane. Some of the numerical methods are listed as follows:

- The method of moments, the surface currents are used to model the microstrip patch, and volume polarization currents in the dielectric slab are used to model the fields in the dielectric slab. An integral equation is calculated for the unknown currents on the microstrip patches and the feed lines and their images in the ground plane.
- The finite-element method, the region of interest is divided into any number of finite surfaces or volume elements depending upon the planar or volumetric structures to be analyzed.
- The spectral domain technique, a two-dimensional Fourier transform along the two orthogonal directions of the patch in the plane of substrate is employed. Boundary conditions are applied in Fourier transform plane. The current distribution on the conducting patch is expanded in terms of chosen basis functions, and the resulting matrix equation is solved to evaluate the electric current distribution on the conducting patch and the equivalent magnetic current distribution on the surrounding substrate surface.
- The finite-difference time domain method, spatial as well as time grid for the electric and magnetic fields are generated over which the solution is required. The spatial discretization along three Cartesian coordinates are taken to be same. The E cell edges are aligned with the boundary of the configuration and H-fields are assumed to be located at the center of each E cell. Each cell contains information about material characteristics.

2.3.3. Rectangular microstrip antenna

A rectangular patch is defined by its length L and width W. For a simple microstrip line, the width is much smaller than the wavelength. However, for the Rectangular Microstrip Antenna, the width is comparable to the wavelength to enhance the radiation from the edges. Since the substrate thickness is much smaller than the wavelength, the Rectangular

Microstrip Antenna is considered to be a two-dimensional planar configuration for analysis.

2.3.4. Design considerations for Rectangular Patch Antennas

A microstrip antenna element can be used alone or in combination with other like elements as part of an array. Usually, the main goal of a design is to achieve specific performance characteristics at an operating frequency. If a microstrip antenna configuration can achieve these overall goals, then the first decision is to select a suitable geometry. A rectangular patch antenna can be design using the procedure described.

- Substrate selection, the first step is to choose a dielectric substrate of appropriate thickness and loss tangent. A thicker substrate, besides being mechanically strong, will increase the radiated power, reduce conductor loss and improve impedance bandwidth. However, it will also increase the weight, dielectric loss, surface wave loss and resonating for substrate thicknesses greater than $0.11\lambda_0$ due to inductive reactance of the probe feed.

  The substrate dielectric constant ε_r has the similar importance as the substrate thickness. A low value of ε_r will increase the fringing field at the patch periphery, and thus the radiated power. Therefore, substrate with $\varepsilon_r \leq 2.5$ are preferred unless a smaller patch size is desired. An increase in the substrate thickness has a similar effect on antenna characteristics as a decrease on the value of ε_r.
- Patch width has a minimum effect on the resonant frequency on the antenna. It affects the input resistance and bandwidth to a larger extent. A larger patch width increases the power radiated and thus gives decreased resonant resistance, increased bandwidth, and increase radiation efficiency. With proper excitation one may choose a patch width W greater than the patch length L without exciting undesired modes. A constraint against a large patch width is the generation of grating lobes in antenna arrays, and a small patch size might be preferred to reduce the real estate requirements. The patch width also affects cross polarization characteristics. The patch width should be selected to obtain good radiation efficiency if real estate requirements or a grating lobe are not overriding factors. It has been suggested that

$$1 < \frac{W}{L} < 2 \tag{2.28}$$

- Radiation pattern and radiation resistance, the radiation patterns of an antenna are of prime importance in determining most of its radiation characteristics which include beam width, beam shape, sidelobe level, directivity, polarization and radiated power. The radiation from the patch can be derived either from the electric fields across the aperture between the patch and the ground plane or form the currents on the surface of the patch conductor. The transmission line model and cavity model employ the aperture field approach. In the transmission line model, two slots at the radiating edges are considered. The cavity model employs four slots along the periphery of the patch. However, the contribution of the non-radiating slots to the radiation pattern can be neglected for approximate calculations.

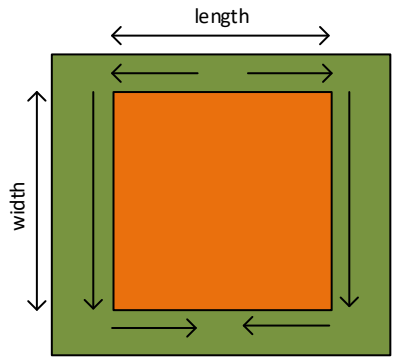

Figure 17: Electromagnetic fields distributions along the periphery in a rectangular microstrip antenna

- Losses and Q factor, the quality factor of a patch antenna needs to be determined to implement the cavity model. It is also useful in determining the VSWR bandwidth of the antenna.
- Bandwidth, it can be defined in a number of ways depending on the characteristics selected.
- Radiation efficiency, the radiation efficiency is defined as the ratio of the radiated power to the input power. The input power gets distributed in the form of radiated power, surface wave power and dissipation in the conductors and dielectric. The dissipated power is generally small for low-loss substrates at microwave frequencies.
- Feed point location, after selecting the patch dimensions L and W for a given substrate, the next task is to determine the feed point (x_0, y_0) so as to obtain a good impedance match between the generator impedance and the input impedance

of the input impedance of the patch element. The input resistance at resonance for the dominant mode can be expressed as

$$R_{in} = R_r \cos^2(\frac{\pi y_0}{L}) \tag{2.29}$$

Where y_0 is the inset distance from the radiating edge, and R_r is the radiation resistance at resonance when the patch is fed at a radiating edge.

Each radiating slot is represented by a parallel equivalent admittance *Y* (with conductance *G* and susceptance *B*). This is shown in figure 18.

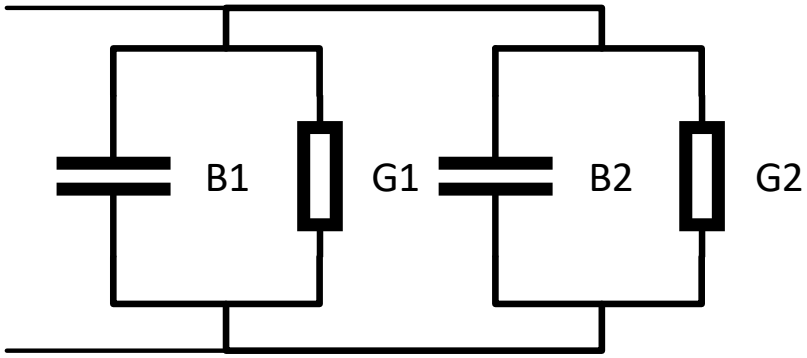

Figure 18: Rectangular microstrip patch and its equivalent circuit transmission-line model

The equivalent admittance of the slot is based on an infinitely wide, uniform slot, is derived and it is given by

$$Y_1 = G_1 + jB_1 \tag{2.30}$$

Where for a slot of finite width W

$$G_1 = \frac{W}{120\lambda_0}\left[1 - \frac{1}{24}(k_0 h)^2\right] \tag{2.31}$$

$$B_1 = \frac{W}{120\lambda_0}[1 - 0.636\ln(k_0 h)] \tag{2.32}$$

Since the slots are identical, its equivalent admittance is

$$Y_2 = Y_1, G_2 = G_1, \;\; B_2 = B_1 \tag{2.33}$$

The conductance of a single slot can also be obtained by using the field expression derived by the cavity model. In general, the conductance is defined as

$$G_1 = \frac{2P_{rad}}{|V_0|^2} \tag{2.34}$$

The radiated power is written as

$$P_{rad} = \frac{|V_0|^2}{2\pi\eta_0}\int_0^{\pi}\left[\sin\frac{\frac{k_0 W}{2}\cos\theta}{\cos\theta}\right]^2 \sin^3\theta \; d\theta \tag{2.35}$$

Therefore, the conductance can be expressed as

$$G_1 = \frac{I_1}{120\pi^2} \tag{2.36}$$

Where $X = k_0 W$

$$I_1 = \int_0^{\pi} \left[\sin \frac{\frac{k_0 W}{2} \cos\theta}{\cos\theta} \right]^2 \sin^3\theta \; d\theta \tag{2.37}$$

$$= -2 + \cos(X) + XS_i(X) + \frac{\sin(X)}{X} \tag{2.38}$$

Asymptotic the previous values are

$$G_1 = \frac{1}{90}\left(\frac{W}{\lambda_0}\right)^2 \qquad W \ll \lambda_0 \tag{2.39}$$

$$G_1 = \frac{1}{120}\left(\frac{W}{\lambda_0}\right)^2 \qquad W \gg \lambda_0 \tag{2.40}$$

The two slots should be separated by $\lambda/2$ where λ is the wavelength in the dielectric (substrate). However, because of fringing the length of the patch is electrically longer than the actual length. Therefore, the actual separation of the two slots is slightly less than $\lambda/2$, the transformed admittance of second slot becomes $\overline{Y_2} = \overline{G_2} + j\overline{B_2} = G_1 - jB_1$ or $\overline{G_2} = G_1,\ \overline{B_2} = -B_1$

Therefore, the total resonant input admittance is real and is given by

$$Y_{in} = Y_1 + \overline{Y_2} = 2G_1 \tag{2.41}$$

Since the total input admittance is real, the resonant input impedance is also real, or

$$Z_{in} = \frac{1}{Y_{in}} = R_{in} = \frac{1}{2G_1} \tag{2.42}$$

The resonant input resistance does not take into account mutual effects between the slots. This can be accomplished by modifying

$$R_{in} = \frac{1}{2(G_1 \pm G_{12})} \tag{2.43}$$

where the plus (+) sign is used for modes with odd resonant voltage distribution beneath the patch and between the slots while the minus (-) sign is used for modes with even resonant voltage distribution. The mutual conductance is defined, in terms of the far-zone fields, as

$$G_{12} = \frac{1}{120\pi^2} \int_0^{\pi} \left[\sin \frac{\frac{k_0 W}{2} \cos\theta}{\cos\theta} \right]^2 J_0(k_0 L sin\theta) \sin^3\theta \, d\theta \tag{2.44}$$

Where J_0 is the Bessel function of the first kind of order zero

Edge feed is used to feed the antenna. The edge impedance *ZA* of the patch antenna is calculated by using

$$Z_{edge} = 90 \cdot \left(\frac{\varepsilon_r^2}{\varepsilon_r - 1}\right)\left(\frac{L}{W}\right)^2 \tag{2.45}$$

- Polarization, the polarization of a rectangular patch antenna is linear and directed along the resonating dimension, when operated in the dominant mode. Large bandwidth patch antennas may operate in the higher mode also. The radiation pattern and polarization for these modes can be different form the dominant mode. Another source for cross-polarization is the fringing field along the non-radiating edges.
- Effects of finite size ground plane, only a finite size ground plane can be implemented. In some applications, for instance in handheld receivers, space is at a premium. Also, for the use of a microstrip antenna as a reflector feed, the ground plane size should be limited. The goal is to reduce the antenna size and the ground plane extension beyond the patch dimensions to a minimum. [10]

2.3.5. Design equations

The value of ε_{eff} is slightly less than ε_r, because the fringing fields around the periphery of the patch are not confined in the dielectric substrate but are also spread in the air, for quick analysis or design, the following approximate equation for e_{eff} could be used

$$\varepsilon_{eff} = \frac{\varepsilon_r + 1}{2} + \frac{\varepsilon_r - 1}{2}\left[1 + \frac{10h}{W}\right]^{-1/2} \tag{2.46}$$

The fundamental TM_{10} mode implies that the field varies one $\lambda/2$ cycle along the length, and there is no variation along the width of the patch. One of the ways to account for the fringing capacitance is to extend the dimensions of the plate outward, and the value of *Ce* can be calculated from:

$$C_{eff} = \varepsilon_0 \varepsilon_r \frac{W_{eff} L_{eff}}{h} \tag{2.47}$$

where, L_{eff} and W_{eff} are the effective dimensions and are equal to:

$$L_{eff} = L + 2\Delta L \tag{2.48}$$

$$W_{eff} = W + 2\Delta W \tag{2.49}$$

The ΔL and ΔW are the extensions along the *L* and *W*, respectively.

$$\Delta L = \frac{h}{\sqrt{\varepsilon_{eff}}} \tag{2.50}$$

Since the effective length of the patch is equal to $\lambda/2$, it can be calculated for a given resonance frequency f_0 as:

$$L_{eff} = \frac{c}{2f_0\sqrt{\varepsilon_{eff}}} \tag{2.51}$$

To calculate ε_{eff}, the value of *W* should be known. For a Rectangular Microstrip Antenna to be an efficient radiator, *W* should be taken equal to a half wavelength corresponding to the average of the two dielectric mediums

$$W = \frac{c}{2f_0\sqrt{\frac{(\varepsilon_r + 1)}{2}}} \tag{2.52}$$

The Bandwidth of the microstrip antenna is inversely proportional to its quality factor Q and is given by

$$BW = \frac{VSWR - 1}{Q\sqrt{VSWR}} \tag{2.53}$$

where VSWR (Voltage Standing Wave Ratio) is defined in terms of the input reflection coefficient Γ as:

$$VSWR = \frac{1 + |\Gamma|}{1 - |\Gamma|} \tag{2.54}$$

$$BW = \frac{2|\Gamma|\sqrt{1 - |\Gamma|^2}}{Q(1 - |\Gamma|^2)} \tag{2.55}$$

The expressions for approximately calculating the bandwidth percentage of the rectangular microstrip antenna in terms of patch dimensions and substrate parameters is given by

$$\%BW = \frac{Ah}{\lambda_0\sqrt{\varepsilon_r}}\sqrt{\frac{W}{L}} \tag{2.56}$$

Where

$$A = 180 \text{ for } \frac{h}{\lambda_0\sqrt{\varepsilon_r}} \leq 0.045 \tag{2.57}$$

$$A = 200 \text{ for } 0.045 \leq \frac{h}{\lambda_0\sqrt{\varepsilon_r}} \leq 0.075 \tag{2.58}$$

$$A = 220 \text{ for } \frac{h}{\lambda_0\sqrt{\varepsilon_r}} \geq 0.075 \tag{2.59}$$

where *W* and *L* are the width and length of the Rectangular Microstrip Antenna.

A narrow band antenna such as a microstrip antenna is limited by impedance match to the connecting transmission line. As operating frequency moves, the patch input impedance increases rapidly, causing large mismatch. The efficiency of the microstrip antenna improves as the impedance mismatch is reduced, which is accomplished by widening the bandwidth. An empirical equation for the bandwidth is [11]

$$BW = 3.77\frac{\varepsilon_r - 1}{e_r^2}\frac{W}{L}\frac{h}{\lambda} \tag{2.60}$$

Where $h \ll \lambda$

The expression for approximately calculating the directivity *D* of the Rectangular Microstrip Antenna is given by

$$D \cong 0.2W + 6.6 + 10\log\left(\frac{1.6}{\sqrt{\varepsilon_r}}\right) dB \tag{2.61}$$

2.4. Microelectromechanical systems

Microelectromechanical systems widely known as MEMS, are systems that consist of small-scale electrical and mechanical components for specific purposes Mainly, they are used in sensors and tv panels because the low power that they need. MEMS are coupled systems since they consist of electrical and mechanical components; the mechanical behavior of MEMS are in general coupled with the electrical behavior.

2.4.1. Transducer

A transducer is a device which converts energy from one form to another. They are often used in automation measurement, and control systems through the use of sensors, where the electrical signals are converted to another physical quantities such as mechanical, force, motion, position, etc. One type of transducers are the mechanical transducers which converts a physical quantity such as movement into an electrical quantity. The other type of transducer is the electrical transducer that converts an electrical magnitude such as a voltages to a mechanical magnitude.

2.4.2. Clamped Free Beam

A beam is a structural element that has the ability to resist forces applied in one of its sides as the figure 19 shows.

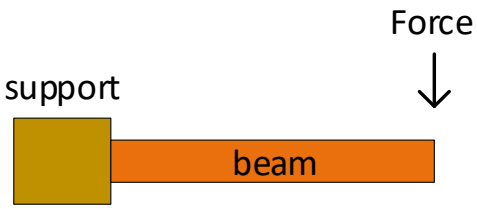

Figure 19: Clamped free beam structure

The simplest structure is the beam simply supported which is a beam supported on the ends then it is free to rotate and have no moment resistance. The fixed beam is a structure that is supported in both ends and restrained from rotation. Over hanging is a simple beam extending beyond its support on one end. Double overhanging is a simple beam with both ends extending beyond its supports on both ends. Cantilever is a clamped free beam fixed only at one end.

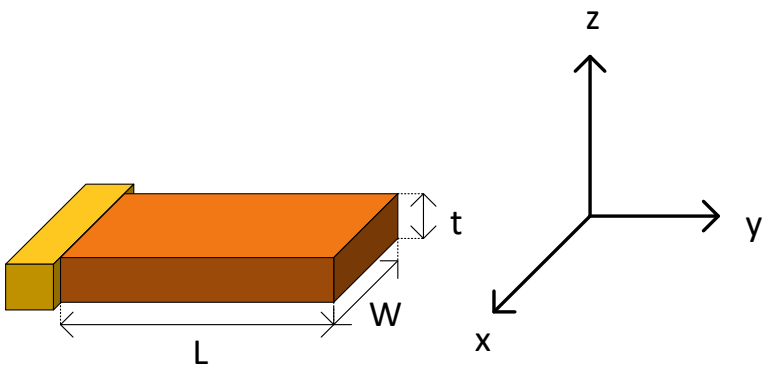

Figure 20: Clamped free beam Cantilever

The dimensions of the structure are shown in figure 20. The length of the cantilever should be longer than the width to allow damped oscillatory response. The thickness of the cantilever is related to the material used. The movement of this cantilever is restricted along the z-axis.

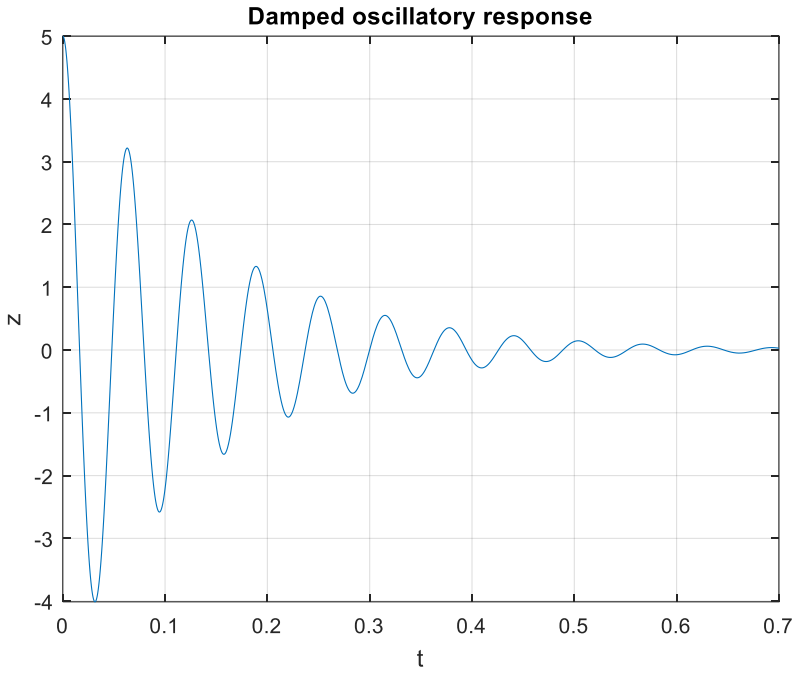

Figure 21: Damped oscillatory cantilever response

The cantilever can be modeled as a spring mass system as shown in the figure 22 where k is the spring constant of the cantilever and m_{eff} is the effective mass of the cantilever.

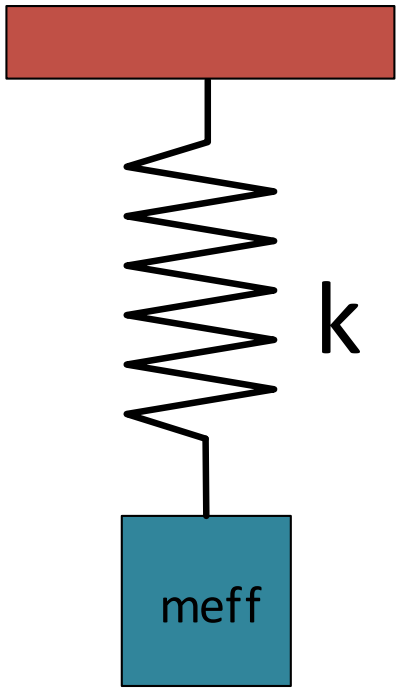

Figure 22:Cantilever model as spring mass system

The spring constant of the cantilever is defined as

$$k = E \cdot W \cdot \frac{t^3}{4 \cdot L^3} \tag{2.62}$$

Where E is the Young's modulus that measure the stiffness of a solid material, typically the value for steel is $200 \cdot 10^9\ Pa$. W, L and t are the width, length and thickness of the cantilever respectively.

The effective mass is strongly related to the type of material used, and it is given as

$$m_{eff} = 0.24 \cdot \rho \cdot W \cdot L \cdot t \tag{2.63}$$

The equation shows that the effective mass is 24% of the total mass. The material density ρ is approximately $8050\ kg/m^3$ for steel material.

The structure performs an angular harmonic frequency response that relates the spring constant and the effective mass as

$$\omega = \sqrt{\frac{k}{m_{eff}}} \tag{2.64}$$

Once the dimensions and characteristics of the clamped free beam is defined, it is possible to define the resonator specifications.

2.4.3. Beam resonator specifications

Ideally, beam resonators are devices that vibrate at a specific frequency with negligible energy loss. In particular, it is desirable for a beam resonator to maintain its frequency of vibration despite changes in temperature, loading conditions, and age. The degree of stability exhibited is given by its electrical parameters

- *Center frequency* is the frequency of resonance of the first mode which is determined by the angular harmonic frequency.
- *Quality factor* (*QF*) is defined as $QF = 2\pi \frac{Energy\ stored\ during\ a\ cycle}{Energy\ lost\ during\ the\ cycle}$, The higher the *QF*, the higher the frequency stability and accuracy capability of the resonator.
- Temperature stability T_f the linear temperature coefficient of frequency, gives the temperature stability: $T_f = \frac{1}{f_R}\frac{df_R}{dT}$. The temperature sensitivity in general will be a function of the expansion coefficient, the spring constant, and the material density, and can be determined for a given resonator design

2.4.4. Fundamentals of microelectromechanical devices

2.4.4.1. Electrostatic Actuation

Some of the concepts required to understand how a microelectromechanical system works refer to the actuation which is the act of transmitting mechanical energy like motion, forces, and work by a device or system on its surroundings, in response to the application of a bias voltage.

Considering a parallel-plate capacitor as the actuator, in which the plates are rigid and constrained from moving, as shown in figure 23 where t represents the thickness of the plate, d is the separation distance between them.

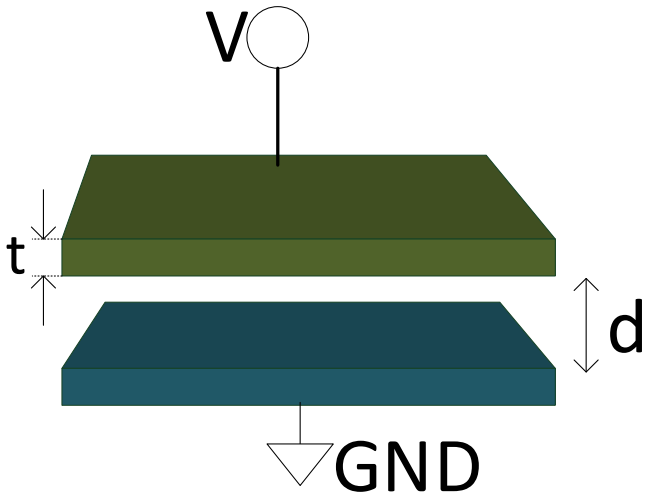

Figure 23: Parallel-plate capacitor as an actuator.

Therefore, the area of the plates is much greater than the separation between them, its capacitance is given

$$C = \frac{\varepsilon A}{d} \tag{2.65}$$

where ε denotes the dielectric permittivity of the medium between the plates, *d* represents the distance separating the plates, and *A* represents the area of the plates. Corresponding to a voltage *V* applied to the capacitor there exists an electrostatic potential energy, given by

$$U = \frac{1}{2} CV^2 \tag{2.66}$$

This potential energy represents the energy required to prevent the oppositely charged parallel plates from collapsing into each other as a result of the coulomb force of attraction. Alternatively, this force may also be expressed as the negative of the gradient in the potential energy between the parallel plates

$$F = -\nabla U = \frac{\varepsilon A V^2}{2d^2} \tag{2.67}$$

This equation quantifies the force that must be applied on the top plate in order to prevent it from collapsing on the bottom plate. It expresses that the force increases linearly with area, quadratically with voltage, and decreases quadratically with the separation between plates.

Then, as the top plate is now free to move, the coulomb force of attraction will make it approach the bottom plate. If the gap *d* decreases, the capacitance, in turn, increases but if the capacitance increases, then the stored energy also increases. This rate of increase in stored potential energy, which is caused by the rate of decrease in gap spacing gives, the instantaneous force of attraction between the plates, which further drives the gap closure.

2.4.4.2. Interdigitated Comb-Drive Capacitor

A key drawback of the parallel-plate capacitor as an actuator is the rapidity with which the force it exerts drops off with increasing gap. This difficulty is overcome by the interdigitated comb-drive capacitor, as shown

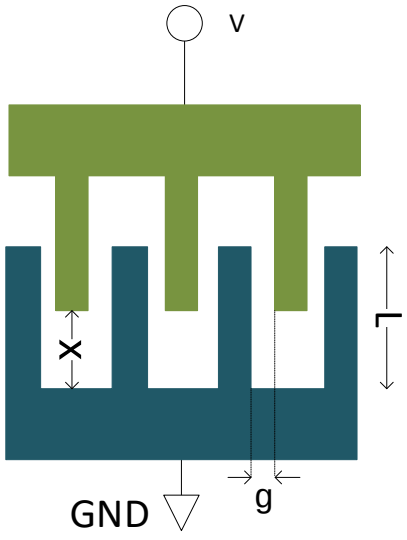

Figure 24: Interdigitated comb drive actuator

The voltage-displacement relationship for the electrostatic comb-drive assumes that both the upper and lower elements are constrained from moving, and that the upper element is held at a fixed voltage *V*. The capacitance for a single tooth face across the gap is given by

$$C_{single} = \frac{\varepsilon A}{g} \tag{2.68}$$

Where the area is given by

$$A = t(L - x) \tag{2.69}$$

Where t is the thickness of the structure, L is the length of the finger and x is the separation distance between the finger and the base. Since each tooth has two sides, it follows that each tooth has two capacitors. For an *n* teeth upper actuator, we have 2*n* capacitors and hence the total capacitance is

$$C_{single} = 2n\frac{\varepsilon t(L - x)}{g} \tag{2.70}$$

The actuation force-displacement relationship

$$F = n\varepsilon\frac{t}{g}V^2 \tag{2.71}$$

A comparison of parallel and comb-drive shows that while the force in a parallel-plate capacitor varies as $\frac{1}{x^2}$, for the comb-drive device the force is constant independent of *x* as long as the degree of comb finger engagement is reasonable. Fringing fields for the comb-drive actuators also give rise to forces out of the plane, which can result in levitation of the actuator away from the substrate.

This structure of transduction keeps moving the movable part along the three directions.

The Figure 25 shows a comb drive, where the bottom electrode can move along the three directions of space and the top electrode is anchored. The plane XY is the substrate plane, t_f is the beam thickness, L_f and w_f are the finger length and width, d_f is the gap between fingers of the different drivers and L_p is the adjacent fingers overlapping length. All these parameters are defined by the layout and the design rules of the technology used to fabricate this device.

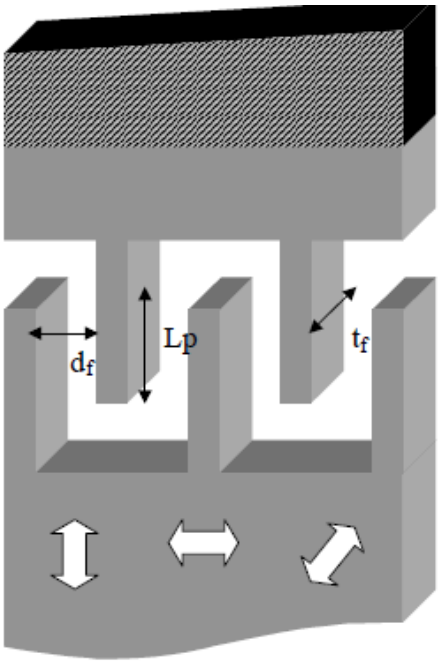

Figure 25: Comb-drive with a mobile part (bottom) and the static part (top). The mobile part can move along the three directions of the space. [12]

The transduction depends on the movement direction of the interdigitated comb; therefore, the structure could be divided into:

- X direction: In-plane gap closing (IPGC) transduction.
- Y direction: In-plane overlap varying (IPOV) transduction.
- Z direction: Out-of-plane gap closing (OPGC) transduction.

Each type of transduction has an expression for the capacitance, the electric force and the energy gain per cycle that depends on its displacement and it corresponds on the direction of the movable part.

Considering the parallel plate studied before the capacitance approximation between the parallel faces of the beams and avoiding the fringing field effects, the capacitance can be calculated between the movable and static parts. Starting from the capacitance value already calculated, we can obtain the electric force magnitude, f_e deriving the expression of the energy stored in the capacitor, U. These expressions depend on the moved distance, along *z-axis*.

a) IPGC comb-driver transduction

$$C(z) = N_g \varepsilon L_p t_f \frac{d_f}{d_f^2 - z^2} \tag{2.72}$$

$$U(z) = Q^2 \frac{d_f^2 - z^2}{2N_g \varepsilon L_p t_f d_f} \tag{2.73}$$

$$f_e(z) = \frac{Q^2 z}{N_g \varepsilon L_p t_f d_f} \tag{2.74}$$

b) IPOV comb-driver transduction

$$C(z) = N_g \varepsilon L_p t_f \frac{(L_p + z)}{d_f} \tag{2.75}$$

$$U(z) = Q^2 \frac{d_f}{2N_g \varepsilon t_f (L_p + z)} \tag{2.76}$$

$$f_e(z) = \frac{Q^2 d_f}{N_g \varepsilon t_f \left(L_p + z\right)^2} \tag{2.77}$$

c) OPGC comb-driver transduction

$$C(z) = N_g \varepsilon L_p \frac{(t_f - |z|)}{d_f} \tag{2.78}$$

$$U(z) = Q^2 \frac{d_f}{2N_g \varepsilon L_p (t_f - |z|)} \tag{2.79}$$

$$f_e(z) = \frac{Q^2 d_f}{N_g \varepsilon t_f \left(L_p + z\right)^2} \tag{2.80}$$

Where *Q* is the initial constant charge inside the capacitor and it can be calculated as the product of the capacitance by the voltage applied, N_g is the number of gaps between adjacent fingers of both drivers. It is important to note that the electrostatic force is proportional to the relative displacement of the mass and, therefore, it acts like a mechanical spring that operates in the opposite direction to the force.

2.4.5. Vertical displacement analysis

The response of a mechanical system to an external force is characterized by three parameters: its mass, *M*, its stiffness, denoted by the "spring constant" *K*, and its damping constant, *D*. In the simplest cases the response may be obtained as a solution to the equation of motion, given by Newton's second law, $\sum F = m \cdot a$. In the cantilever beam with possible displacement in the *z* direction and neglecting gravity, if an external force is applied, the equation of motion takes the form

$$M\ddot{z} + D\dot{z} + Kz = F \tag{2.81}$$

where the dot denotes derivative with respect to time. This equation is known as the differential equation of motion of a single-degree-of-freedom system. It states that the

motion z elicited by an applied force F, is the result of the balance between the applied force, on the one hand, and the resultant of the impulsive motion, $M\ddot{z}$, the viscous damping force experienced by the system once it starts to develop a speed, $D\dot{z}$, and the "spring" force Kz which commands the system to return to its equilibrium position.

The system can be further simplified by adopting the idealization that there is no viscous damping. The solution then is given by

$$M\ddot{z} + Kz = 0 \tag{2.82}$$

which has a general solution as

$$z = Asin\left(\sqrt{\frac{K}{M}} \cdot t\right) + Bcos\left(\sqrt{\frac{K}{M}} \cdot t\right) \tag{2.83}$$

where *A* and *B* are arbitrary constants. This represents temporal evolution of the beam's spatial shape under undamped conditions. So, taking into account the general form of the sinusoidal function where the angular frequency is multiplied by the dependent variable, we can infer that the natural frequency of the system is given by

$$f = \frac{1}{2\pi}\sqrt{\frac{K}{m_{eff}}} \tag{2.84}$$

Finally, the pull in voltage that collapse the system is given by

$$V_p = 2 \cdot \frac{\sqrt{\left(k \cdot \frac{s_0^3}{\varepsilon \cdot A_{ee}}\right)}}{3\sqrt{3}} \tag{2.85}$$

Where k is the spring constant, s_0 is the distance between plates, A_{ee} is the area of the capacitor ε is the vacuum permittivity.

3. Analysis and Design

Based on the theory studied in the previous chapter, where it is explained about performance in microstrip antennas and microelectromechanical systems, this chapter shows the analysis and design for the implementation of the system.

As starting point a mathematical model related to a dipole cantilever configuration was analyzed. To understand how the system works, it was necessary to get previous background in mechanical systems, mainly in mass spring systems

3.1. Proposed System

The purpose of this project is to use microelectromechanical systems through a cantilever beam structure to convert the energy transmitted by the RF antenna into mechanical energy that produce vibrations in its structure. So, as it is explained in last chapter when a voltage is applied between two cantilever or conductors like parallel plates, an electrostatic force appears and it induces displacement of non-fixed edge.

The proposed system is shown in the figure 26 where In the transmission side the RF generator, that is used to generate the carrier signal at high frequency, and the low frequency generator, that produce the modulating signal, are located as the result of mixing both signals the amplitude modulated signal is obtained and transmitted through rectangular microstrip antenna to the receiver. In the receiver, the same antenna receives the electromagnetic waves and it transfer the signal to the connectors as the input signal. This input signal is sent to the clamped free beam to start the demodulation process.

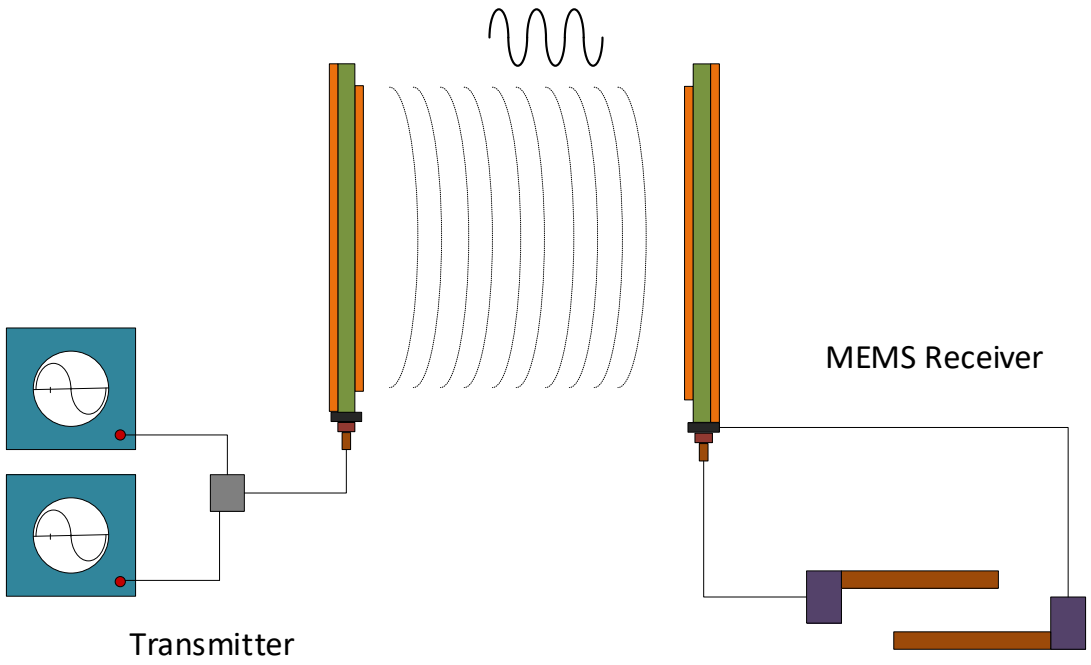

Figure 26: System`s diagram proposed.

3.2. Antenna design

The initial requirements are a given by the constraints related to the power source and the frequency operation.

- The transmission power available comes from the generator and the amplifier is up to 44 dBm
- The frequency of operation is 1 GHz

A design constraint related to the available materials was taken into account as part of the analysis. The analysis includes two types of material FR4 and ROGERS 3010.

First of all, it is good to mention that

- FR4 refers to a grade of material rather than a material, which is a composite material for glass-reinforced epoxy laminate material. FR-4 is made up of woven fiberglass cloth with an epoxy resin binder that is flame resistant.
- Rogers is a company that manufactures the laminate materials that are used to make circuit boards.

A comparison between them is shown in table 1

FR4	ROGERS
Perform better at low frequency, the best at 1 MHz	Perform better at high frequencies
Dissipation factor: 0.014 means this material suffer less signal loss	ROGERS 3010 dissipation factor: 0.0023 means this material suffer less signal loss
Dielectric constant about 4.5	Dielectric constant about 10.2
Temperature management, high variation	Temperature management, less variation

Table 1: Substrate materials comparison

As you can see in table 1, the best material that performs the system is ROGERS 3010 because it works better at high frequencies and it has a greater dielectric constant compared to FR4, therefore the microstrip area would be smaller.

Using equations described in section 2.3.5 where the design equations of a rectangular microstrip antenna are described, table 2 shows dimensions and some characteristics of the antenna proposed

Parameters	
Frequency	1 GHz
Permittivity ε_r	10.2
Substrate height	1.28 mm
Tangent loss	0.022
Width	6.34 cm
Length	4.7 cm
Effective Permittivity $\varepsilon_{r_{eff}}$	9.73
Delta Length	0.6 mm
Effective Length	4.81 cm
Ground Plane Length	5.5 cm
Ground Plane Width	7.1 cm
Directivity	3.6109 (5.6 dB)
Input resistance	$6.22x10^4$ Ω
Bandwidth	0.0251 (2.51%)
Feedline width	1.22 mm

Table 2: Rectangular patch antenna characteristics

Based on, the previous values obtained, the feedline width was obtained using the online calculator (https://www.emtalk.com/mscalc.php).

The simulation was done using Feko software version 2019. (CadFeko and PostFeko). In Figure 27 shows the substrate configuration used to simulate ROGERS 3010

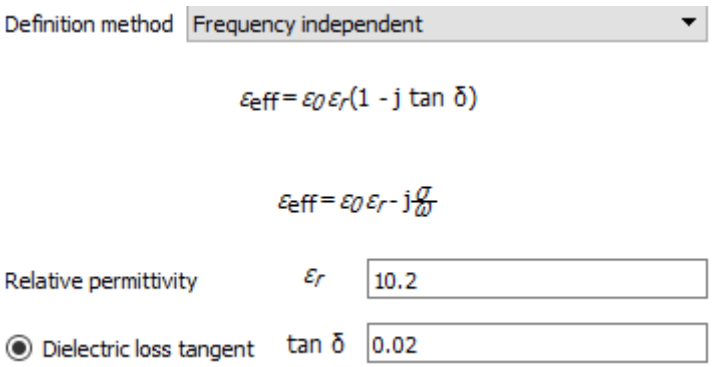

Figure 27: Substrate configuration ROGER 3010

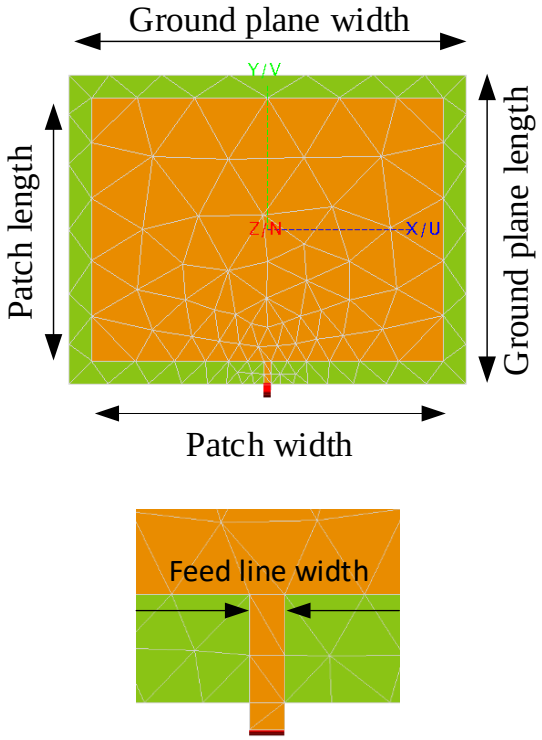

Figure 28: Feko Antenna dimensions

The Figure 29 shows the reflection coefficient diagram where the resonant frequency is set at 1.00513 GHz and the reflection coefficient is -17.8593 dB.

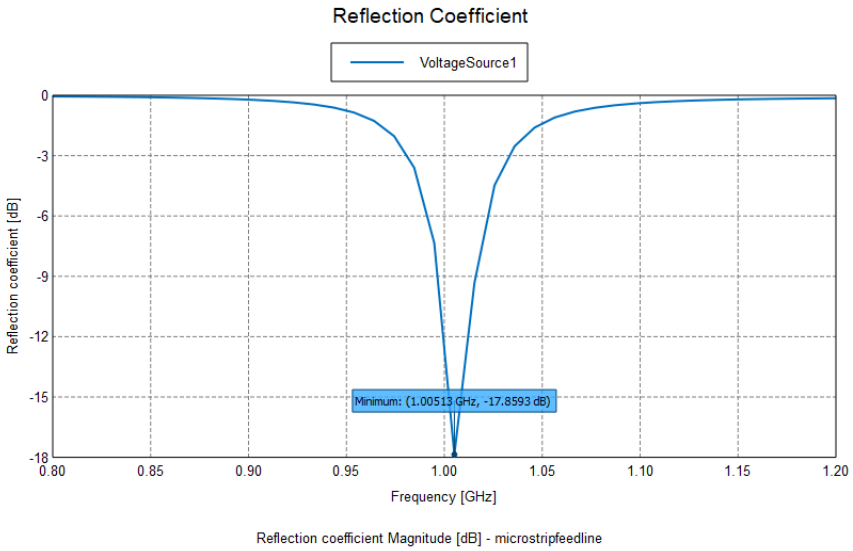

Figure 29: Antenna Reflection coefficient

So, the reflection mismatch efficiency is

$$e_r = 1 - |S|^2 \tag{3.1}$$

$$e_r = 1 - 0.1279^2 = 0.922$$

The available power given as a design parameter is 44 dBm (25.12 W), so the accepted power can be calculated as

$$W_a = W_s e_r \tag{3.2}$$

$$W_a = 25.12 \cdot 0.922 = 23.16W(43.65dBm)$$

The impedance of the antenna simulated is $62.438 - i \cdot 7.28\,\Omega$. The figures 30 and 31 show that the antenna is closer to the impedance reference of 50 ohms. Thereby, the radiation efficiency can be calculated taking into account that the radiation resistance is equal to the reference and the antenna resistance is $e_{cd} = \frac{R_r}{R_a} = \frac{50}{62.438} = 0.8$

The effective power transmitted is given by the multiplication of the accepted power, the mismatch efficiency and the radiation efficiency.

$$W_r = W_a e_{cd} \tag{3.3}$$

$$W_r = 23.16 * 0.8 = 18.53\,W\ (42.68\,dBm)$$

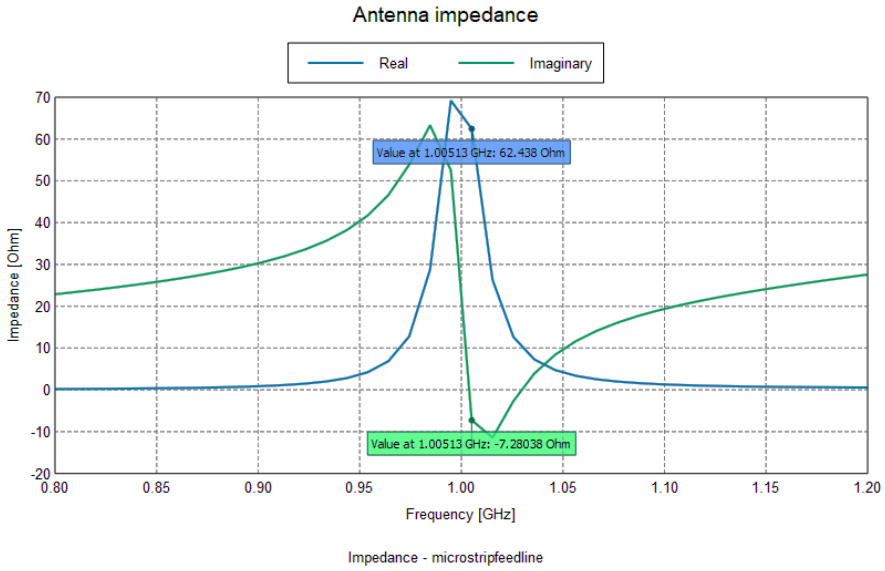

Figure 30: Antenna impedance diagram at 1.00513 GHz

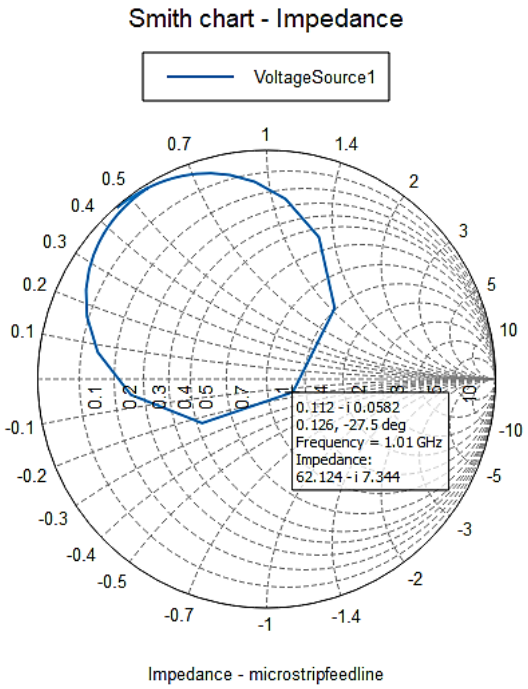

Figure 31: Smith chart diagram of the antenna at 1.00513 GHz

The radiation pattern of the antenna is shown in the figure 32, the maximum value in directivity is set about 3.04 dBi which comparing to the theoretical, the value obtained is close. It shows a directional pattern at tilt angle $\varphi = \pi/2$

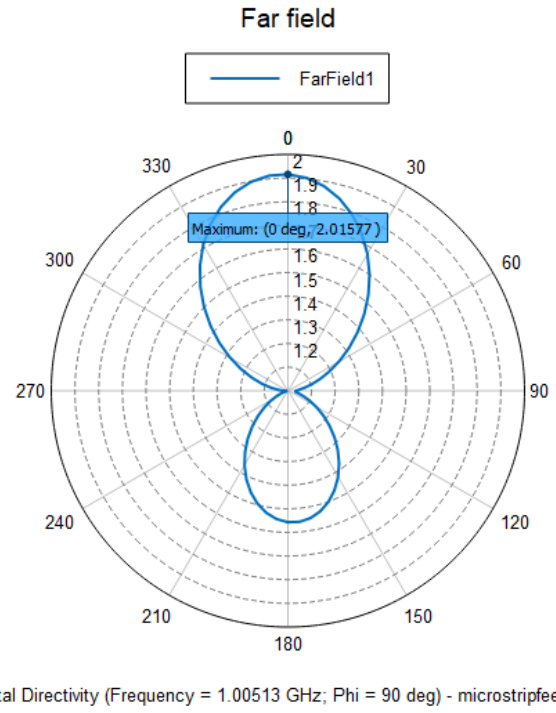

Figure 32: Radiation pattern of the antenna at 1.00513 GHz

Based on the parameters already calculated about power transmission and directivities, it is possible to obtain the minimum separation distance between two antennas as

$$r = 2 \cdot \lambda = 2 \cdot 0.3 = 0.6\, m \tag{3.4}$$

So, the minimum power received at that distance is given by

$$W_L = W_R D_T D_R \left(\frac{\lambda}{4\pi r}\right)^2 \tag{3.5}$$

$$W_L = 18.53 \cdot 3.6 \cdot 3.6 \cdot \left(\frac{0.3}{4\pi \cdot 0.6}\right)^2$$

$$W_L = 0.38\, W\ (25.8\, dBm)$$

Where λ is the wavelength and r is the separation distance between the antennas.

3.3. Parallel Cantilever

As the theory shows, a parallel beam system (cantilever) works as a spring mass mechanical system. Basically, applying a voltage between the terminals of the cantilevers, it is possible to generate an electrostatic force that moves the structure in its characteristic frequency; this frequency depends strongly on its physical dimensions.

In Figures 33 and 34 show the structure of the cantilever. The structure is fixed in each of their ends, so the vibration in z-axis are limited in movement. In figure 34 the structure shows the effective area, which is defined by the product of the overlap length and the width of the cantilever. To simplify the area in the design the overlap length is equal to the width so the area is w^2.

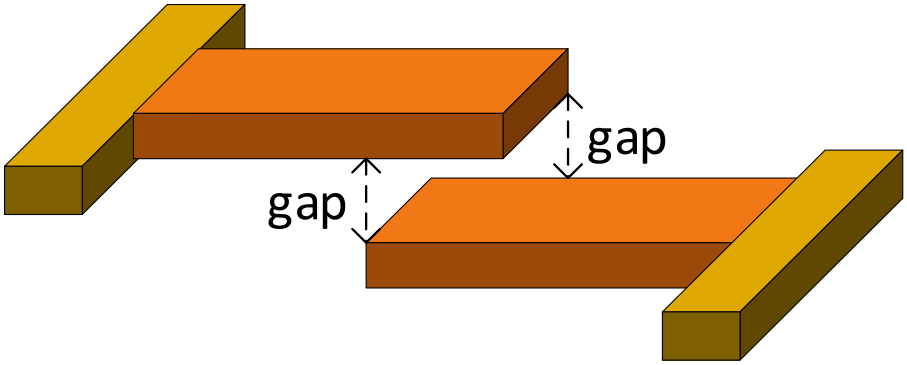

Figure 33: Geometry of the cantilever 3D view

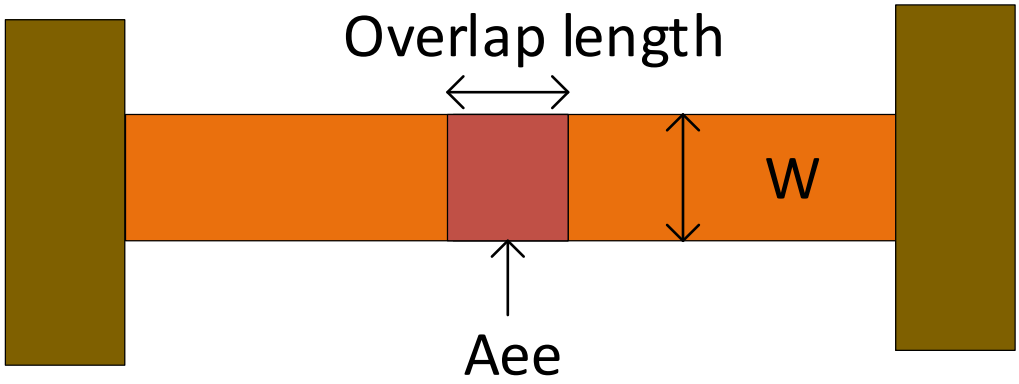

Figure 34: Effective area of the cantilever

3.3.1. Open circuit voltage calculation

As the beginning of the analysis, it is necessary to determine the open circuit voltage present in the receiver antenna. It could be calculated using the equation

$$V_{OC} = l_{ef} \cdot E_i \tag{3.6}$$

Therefore, the effective length of the antenna is calculated from the effective area of the antenna as

$$A_{ef} = \frac{\lambda^2}{4\pi} D \tag{3.7}$$

$$A_{ef} = \frac{0.3^2}{4\pi} \cdot 3.02 = 0.022\ m^2$$

Where the D is the directivity of the antenna and lambda is wavelength in meters. So, taking into account the antenna resistance R_a in the equation of the effective length, we have

$$l_{ef} = \sqrt{4 \cdot R_a \cdot \frac{A_{ef}}{120\pi}} \tag{3.8}$$

$$l_{ef} = \sqrt{4 \cdot 62.438 \cdot \frac{0.022}{120\pi}} = 0.12\ m$$

The electric field strength at a specific distance is calculated from measurements of the power delivered from the transmitting antenna and a knowledge of the gain of the antenna as a function of frequency and distance to the field point. The electric field *E* on the boresight axis of the transmitting antenna is [13]

$$E = \frac{\sqrt{60 W_r \cdot D}}{r} = \frac{7.75\sqrt{W_r D}}{r} \tag{3.9}$$

Where r is the distance between antennas. So, the equation above was programmed in a Matlab script, it helps us to estimate the electric field at different separation distances between antennas as is shown in the figure 35. The figure shows that the decrement of the electric field is almost exponential, and it decrease quickly.

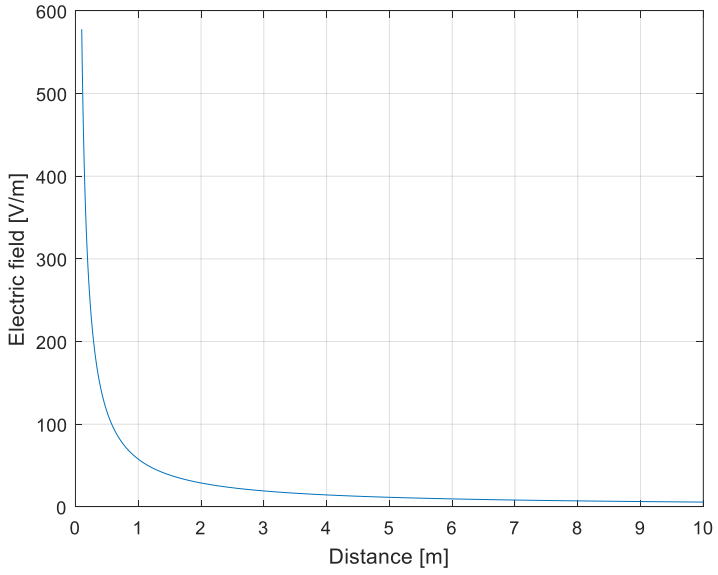

Figure 35: Electric field at given distances from 0 to 10 meters

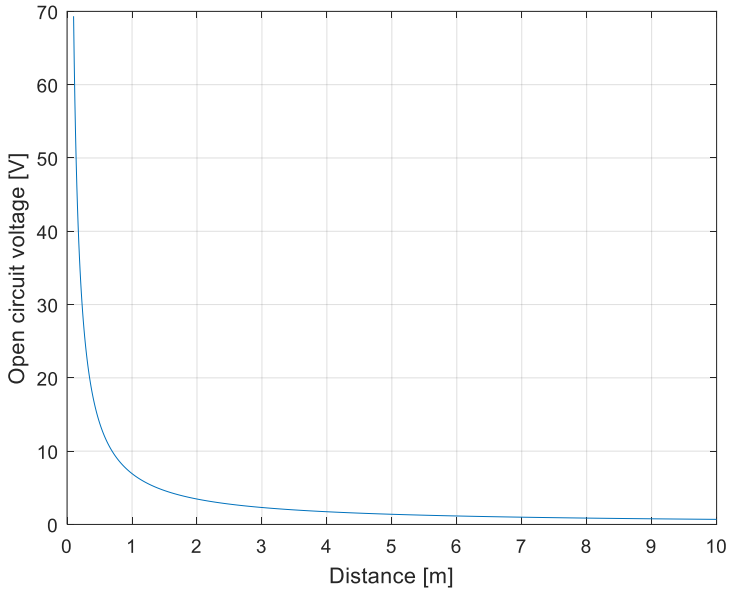

Figure 36: Open circuit voltage at given distances from 0 to 10 meters

The Figure 36 shows a similar response in the open circuit calculation, it is decreasing exponentially with the distance. It can help us to determine the best separation distance between antennas. Because the dimensions of the cantilever beam are small, the pull in voltage described in the previous chapter would be dramatically difficult to manage.

Finally, the equivalent circuit of the antenna is connected to the beam cantilever as it is shown in figure 37. It models in the characteristic circuit of an antenna where the cantilever is considered as a variable capacitance.

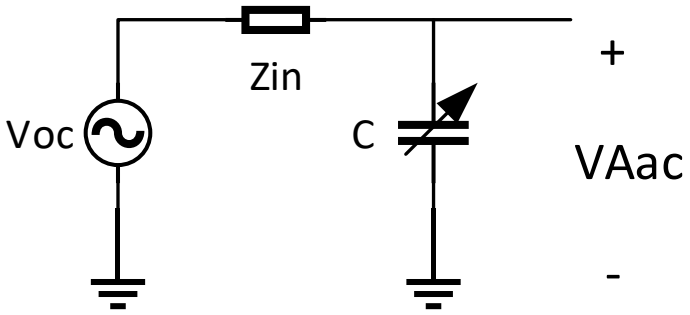

Figure 37: Equivalent circuit antenna and beam cantilever

In order to solve this circuit a voltage divider equation is proposed

$$VAac = \frac{V_{oc}}{\|1 - w \cdot X_A \cdot C + i \cdot R_A \cdot C \cdot w\|} \tag{3.10}$$

$$VAac = \frac{1}{\sqrt{(1 - w \cdot X_A \cdot C)^2 + (R_A \cdot C \cdot w)^2}} \cdot V_{oc} \quad (3.11)$$

Where $VAac$ is the voltage in the cantilever, C is the capacitance of the cantilever, X_A is the imaginary part of the antenna input impedance, R_A is the real part of the antenna input impedance and w is the frequency operation of the antenna.

3.3.2. Analysis of cantilever dimension

The initial dimensions and parameters of the cantilever proposed in table 3 were taken from previous projects where these dimensions were used to stimulate a dipole antenna to works as a beam cantilever.

Parameters	
Length	83 mm
Width	5 mm
Thickness	136 μm
Gap	50 μm
Frequency	16 Hz
Capacitance	4.5 pF

Table 3: Initial parameters of the cantilever

After doing some analysis of the cantilever dimensions, and trying to reduce them to achieve a frequency which performs better to musical note frequencies as the table 5 shows, a scale factor from 0.1 to 1 (step 0.01) was analyzed. This factor was taken as a proportional product among the initial parameters.

The table 4 shows, the dimension that performs better starts from 0.16 times in the scale factor, this means that if they are reduced up to 0.01 times the musical notes ranges can be obtained. On the contrary, the dimensions are practically related to the technology used, so at the end to obtain a gap smaller than 3 µm could be difficult.

SF	Length [mm]	Width [mm]	Thickness [μm]	Gap [μm]	Frequency [Hz]	Cap [F]
0,06	4,98	0,30	8,16	3,00	266,40	3,09E-13
0,07	5,81	0,35	9,52	3,50	228,34	3,41E-13
0,08	6,64	0,40	10,9	4,00	199,80	3,87E-13
0,09	7,47	0,45	12,2	4,50	177,60	4,34E-13

0,1	8,30	0,50	13,6	5,00	159,84	4,82E-13
0,11	9,13	0,55	15,0	5,50	145,31	5,30E-13
0,12	9,96	0,60	16,3	6,00	133,20	5,77E-13
0,13	10,8	0,65	17,7	6,50	122,95	6,25E-13
0,14	11,6	0,70	19,0	7,00	114,17	6,72E-13
0,15	12,5	0,75	20,4	7,50	106,56	7,20E-13
0,16	13,3	0,80	21,8	8,00	99,90	7,67E-13

Table 4:Dimensions base on scale factor

Musical note	Frequency [Hz]
Do	261.626
Re	293.665
Mi	329.628
Fa	349.228
Sol	391.995
La	440
Si	493.88

Table 5: Musical notes frequency

3.3.3. DC voltage applied to the cantilever

The vertical deflection of the beam cantilever for the case of applying continuous voltage shows the damped oscillatory movement so at the end the cantilever stays in repose. Due to proportionality in the electrostatic force as $F_e \propto V^2$, the continuous voltage forces the structure to oscillate but it is not enough to obtain a continuous oscillation. This kind of response is identical to the spring mass system studied before.

It is important to stablish that the system response is due to the movements of both cantilevers in opposite direction cause the forces applied, consequently, the electrostatic force applied it is half. The voltage in the cantilever which is labeled as ac voltage shows some variations respect to the open circuit voltage due to it works as a variable capacitance.

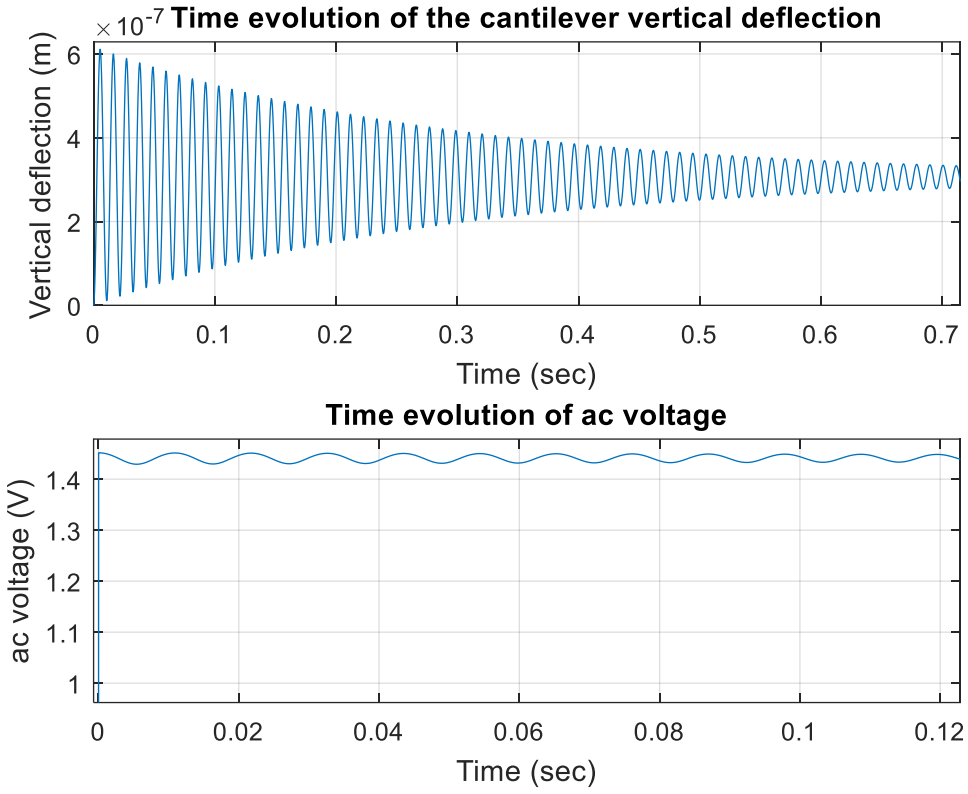

Figure 38:Beam cantilever response at DC voltage

3.3.4. AC voltage applied to the cantilever

Defining the sinusoidal input voltage as

$$V(t) = V_{OC} \sin(2 \cdot \pi \cdot f \cdot t) \tag{3.12}$$

Where the amplitude of the signal takes the value of the open circuit voltage and f is the natural frequency of the cantilever structure.

Getting the values from table 4 where the beam cantilever frequency is set to 99.9 Hz, the figure 39 shows the cantilever dimensions and stablish the initial gap as 8 micrometers.

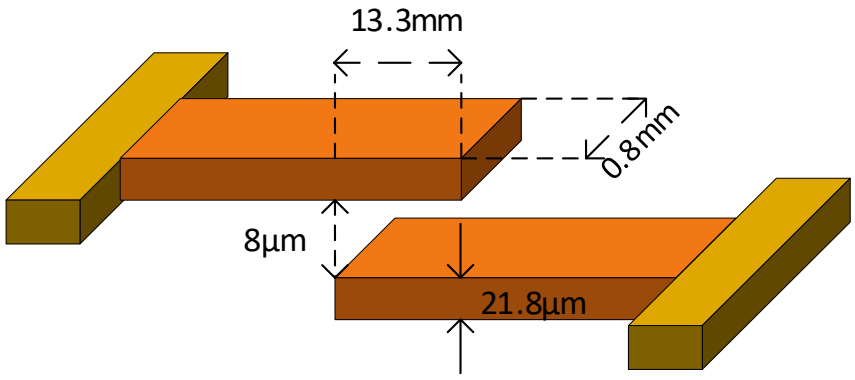

Figure 39: Cantilever dimension at 0.16 scale factor

The output signal is shown in the figure 40, it shows the vibrations due the spring mass model explained in previous chapter where the vertical movement of a cantilever is explained. In the output signal is possible to notice that the stability takes time due to the initial forced movement of the cantilever but after approximately 0.8 seconds the response is actually the same as the input.

The electrostatic force applied to the structure is

$$F_{ee} = 0.25 \cdot \varepsilon \cdot \frac{A_{ee}}{s_0} \cdot (V_{oc} \cdot \sin(w_m \cdot t))^2 \tag{3.13}$$

$$F_{ee} = 0.25 \cdot \varepsilon \cdot \frac{A_{ee}}{s_0} \cdot V_{oc}^2 \cdot \sin^2(w_m \cdot t) \tag{3.14}$$

$$F_{ee} = 0.25 \cdot \varepsilon \cdot \frac{A_{ee}}{s_0} \cdot \frac{V_{oc}^2}{2} \cdot (1 - \cos(2 \cdot w_m \cdot t)) \tag{3.15}$$

The figure “time evolution of ac voltage” shows the cantilever voltage along the time stablished by the simulation, the voltage variation in the beam cantilever is due to the vibration and the variation of the gap.

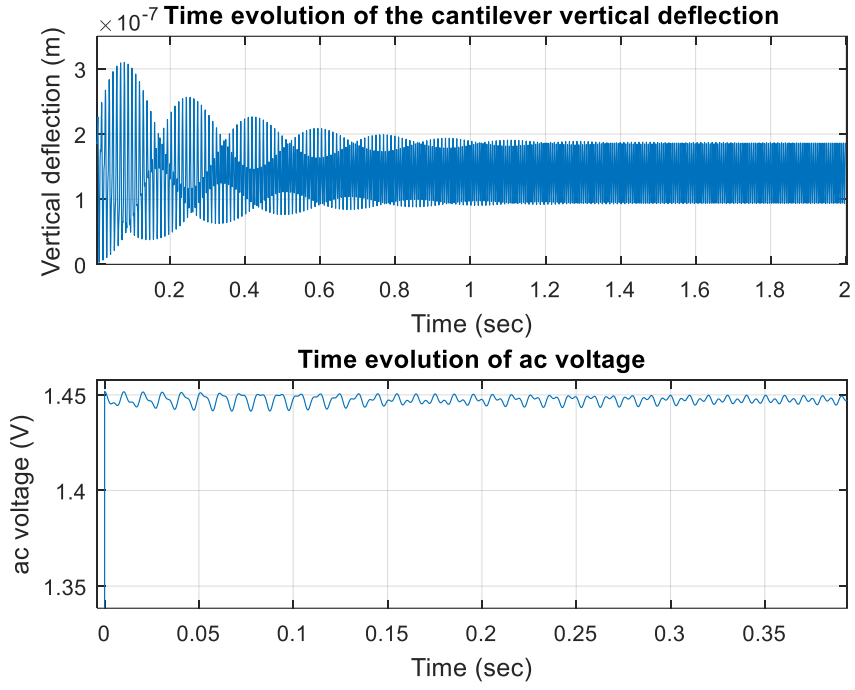

Figure 40: Beam cantilever response sinusoidal input signal

3.3.5. Amplitude modulated signal applied to the cantilever

The case of an amplitude modulated input signal was studied, the equation 2.6 was used to define the input signal as

$$V_{AM} = E_C \cdot (1 + m \cdot \sin(w_m \cdot t)) \cdot \sin(w_C \cdot t) \tag{3.16}$$

Where $E_C = V_{oc}$, the index modulation is set to $m = 0.8$ as a parameter design, w_m is the angular frequency of the cantilever and w_C is the angular frequency of the carrier. The voltage applied to the structure can be replaced into the electrostatic force as

$$F_{ee} = 0.25 \cdot \varepsilon \cdot \frac{A_{ee}}{s_0^2} \cdot (V_{AM})^2 \tag{3.17}$$

As the cantilever structure has the ability to get vibration at the frequency that it is designed. So, the amplitude modulated voltage applied into the electrostatic force has the components of the DC voltage and the voltage at the modulating frequency w_M. The equation can be simplified just taking into account those terms.

$$V_{AM_{DC}} = \frac{V_{oc}^2}{4} \cdot (2 + m^2) \tag{3.18}$$

$$V_{AM_{w_M}} = V_{oc}^2 \cdot m \cdot \sin(w_M \cdot t) \tag{3.19}$$

Therefore, the electrostatic force can be expressed as

$$F_{ee} = 0.25 \cdot \varepsilon \cdot \frac{A_{ee}}{s_0^2} \cdot \frac{V_{oc}^2}{4} \cdot (2 + m^2 + 4 \cdot m \cdot \sin(w_M \cdot t) + m^2 \cdot \cos(2 \cdot w_M \cdot t)) \tag{3.20}$$

The figure 41 shows the output signal obtained where it is possible to see in the vertical deflection a similar wave as the modulating signal, and the variations in the cantilever shows a sinusoidal fluctuation similar to the modulating signal.

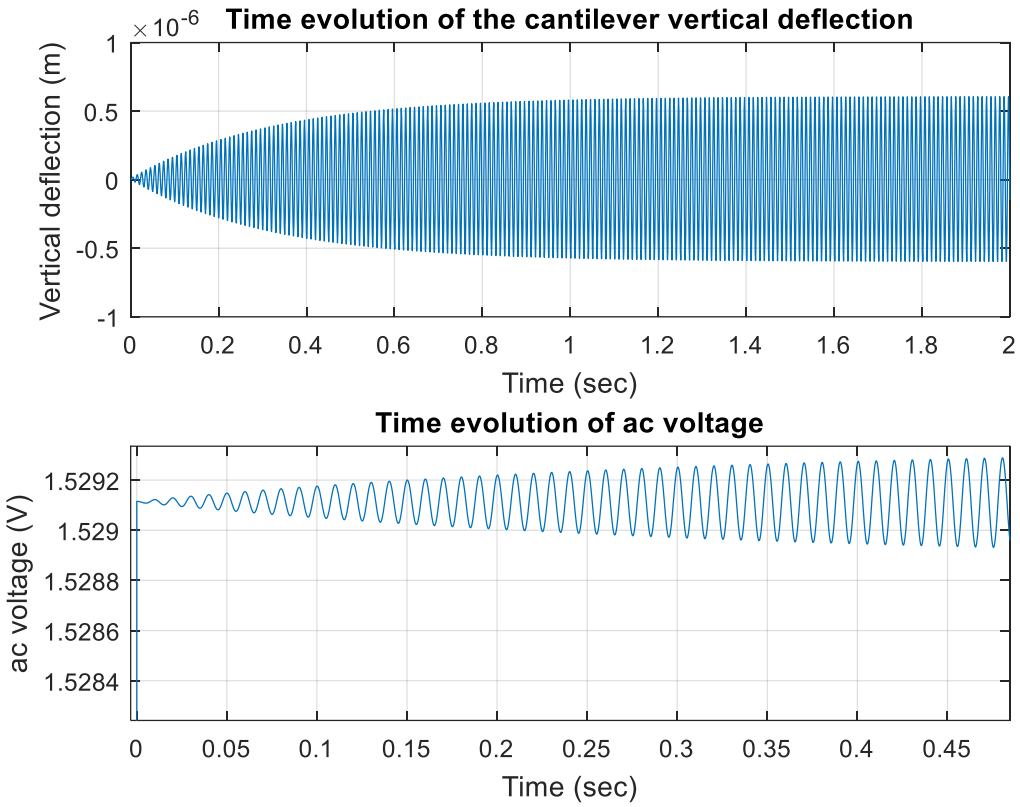

Figure 41: Beam cantilever response at amplitude modulated signal

Doing a zoom in the figure of the vertical deflection it is possible to see the period of the signal which is 0.01 seconds (100 Hz), and comparing to the modulating frequency it is the same.

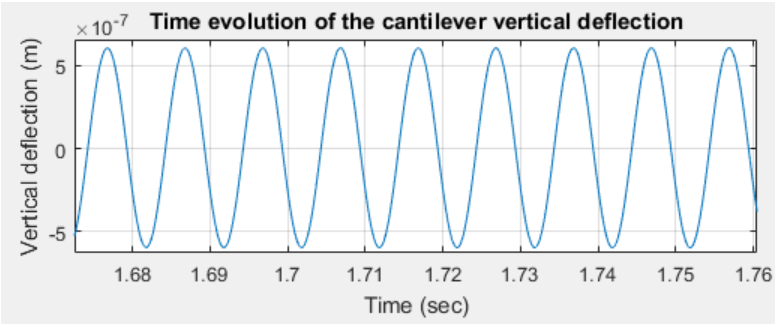

Figure 42: Amplitude modulated response as the output signal of the cantilever

3.3.6. Sound pressure level produced in the cantilever

As an application of the receiver, the analysis of the sound pressure level in the output was done. One of the goals proposed in the chapter 1 was to determine if the vertical displacement obtained by the vibrations are enough to produce audible sound. Thereby, the concept of the sound pressure level as the local pressure deviation from the ambient atmospheric pressure, caused by a sound wave stablish the density of the air as

$\rho_{air} = 1.225\ kg/m^3$, the sound velocity of the air in the vacuum as $c_{air} = 343\ m/s$, the rms velocity of the sound as the product of the angular modulating frequency and the amplitude and the minimum level of sound pressure as

$$v_{rms} = w_M * A \tag{3.21}$$

$$P_0 = 2 * 10^{-5}\ Pa \tag{3.22}$$

Once the variables were described, it is possible to determine the sound pressure level as

$$P_{rms} = \rho_{air} * c_{air} * v_{rms} \tag{3.23}$$

$$SPL = 20 * \log\left(\frac{P_{rms}}{P_0}\right)\ dB \tag{3.24}$$

The figure 42 shows the amplitude of the output signal which is approximately $1.18\ \mu m$. Consequently, the sound pressure level in the source is calculated using the equations 3.22 and 3.23

$$P_{rms} = 1.225 \cdot 343 \cdot 2\pi \cdot 100 \cdot 0.6 \cdot 10^{-6} = 0.158\ Pa$$

$$SPL = 20 \cdot \log\left(\frac{0.158}{2 \cdot 10^{-5}}\right) = 77.95\ dB$$

The sound pressure level calculated shows a higher level of sound comparing to the minimum level defined.

To estimate the value of the sound pressure level at a given distance, the following equation can be used

$$P(z) = \frac{R_0 \cdot P_0}{z} \tag{3.25}$$

Where R_0 is the Rayleigh length, it is defined as $R_0 = A_{ee}/\lambda$, P_0 is the sound pressure at the source and z is the sound propagation distance; where A_{ee} is the overlapping area of the cantilever and λ is the sound wavelength.

The figure 43 shows the sound pressure level along a range of distances from 0 to 5 centimeters. It is possible to determine that it decreases asymptotically as the distance increase, but taking into account that the minimum sound pressure value as the reference of 0 dB, the sound pressure level produced by the cantilever is higher than the minimum established up to 0.1 centimeters of separation distance with the source, approximately. Due to the proportionality of the overlapping area between cantilevers is $0.64\ \mu m^2$, the Rayleigh length is affected.

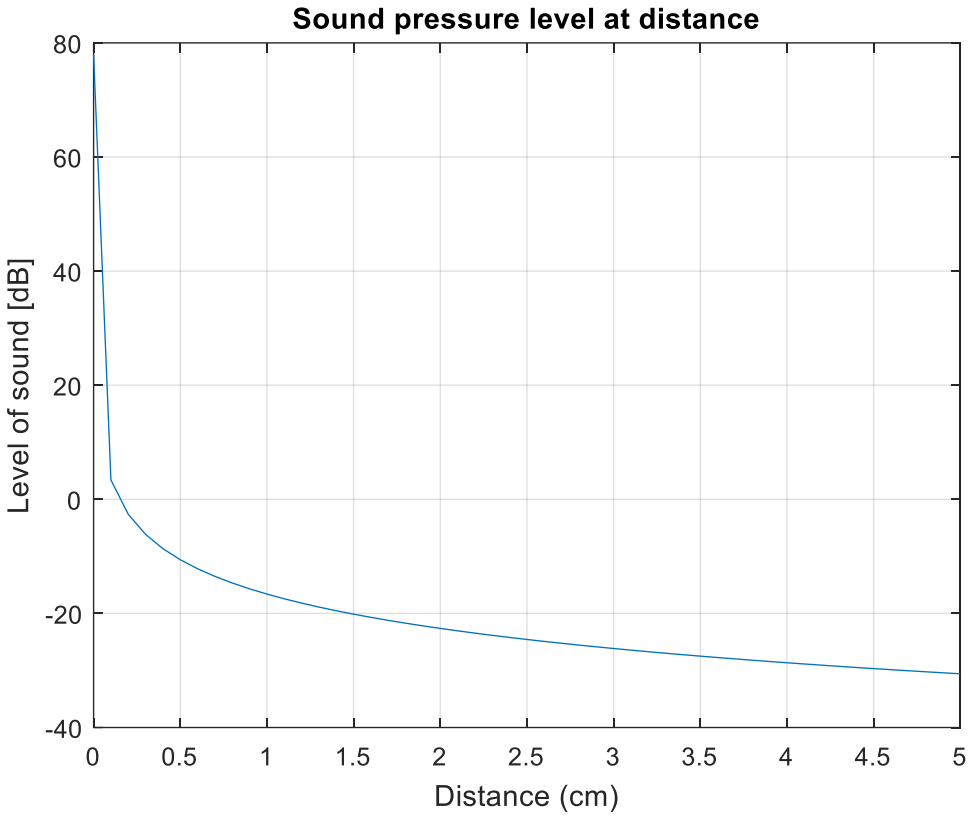

Figure 43:Sound pressure level from 0 to 5 cm in beam cantilever

3.4. Comb cantilever

The functionality of comb capacitor is shown in section 2.4.4.2. Its capacitance is related to the number of gaps that could contain into a specific width.

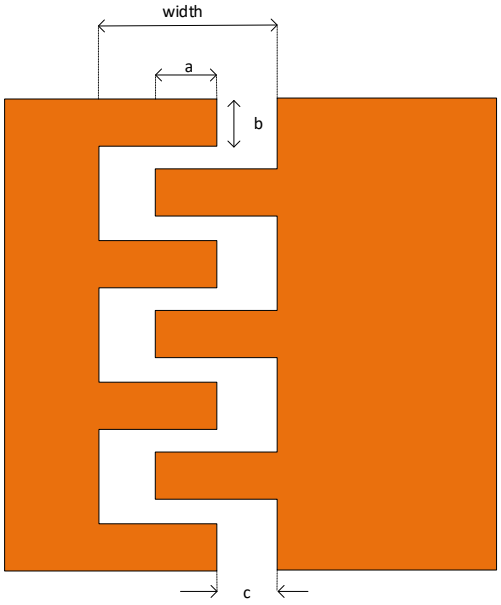

Figure 44: Comb cantilever structure

The figure above shows the characteristic dimensions of the comb cantilever proposed, where

- a is the finger length
- b is the finger width
- c is the separation between fingers

In order to obtain a mathematical model of the structure, some design parameters were set

- The width of the interdigitated cantilever is set to 0.8 mm,
- The finger overlapping length L_p described in Comb cantilever section, is set to 80% of the width
- The finger width and the gap width are identical.

To calculate the number of gaps, it is necessary to define that the total width of the cantilever is proportional as the width of one of the fingers as

$$N_g = \frac{W}{2 \cdot b} \tag{3.26}$$

SF	Width	0.01	0.02	0.03	0.04	0.05	0.06	0.07	0.08	0.09	0.1
	mm	Number of gaps									
0,01	0.05	3	1	1	1	1	0	0	0	0	0
0,02	0.1	5	3	2	1	1	1	1	1	1	1
0,03	0.15	8	4	3	2	2	1	1	1	1	1
0,04	0.2	10	5	3	3	2	2	1	1	1	1
0,05	0.25	13	6	4	3	3	2	2	2	1	1
0,06	0.3	15	8	5	4	3	3	2	2	2	2
0,07	0.35	18	9	6	4	4	3	3	2	2	2
0,08	0.4	20	10	7	5	4	3	3	3	2	2
0,09	0.45	23	11	8	6	5	4	3	3	3	2
0,1	0.5	25	13	8	6	5	4	4	3	3	3
0,11	0.55	28	14	9	7	6	5	4	3	3	3
0,12	0.6	30	15	10	8	6	5	4	4	3	3
0,13	0.65	33	16	11	8	7	5	5	4	4	3
0,14	0.7	35	18	12	9	7	6	5	4	4	4
0,15	0.75	38	19	13	9	8	6	5	5	4	4

0,16	0.8	40	20	13	10	8	7	6	5	4	4

Table 6: Number of gaps between finger width and total width

The table above shows the total number of gaps based on the total width and the width of each finger which is in the range of 0.01 to 0.1 mm. Using, 10 µm as the width of the gap and based on the parameter design stablished as $w_f = w_g$, the maximum number of gaps for 0.8 mm of total width is 40 which means a maximum capacitance of

$$C_{max} = N_g \cdot \varepsilon \cdot L_p \cdot \frac{t_f}{w_f} \tag{3.27}$$

$$C_{max} = \frac{w}{2 \cdot w_f} \cdot \varepsilon \cdot 0.8 \cdot w \cdot \frac{t_f}{w_f} \tag{3.28}$$

$$C_{max} = 0.4 \cdot \left(\frac{w}{w_f}\right)^2 \cdot \varepsilon \cdot t_f \tag{3.29}$$

$$C_{max} = 0.4 \cdot \left(\frac{0.8}{0.01}\right)^2 \cdot 8.85 \cdot 10^{-12} \cdot 21.76 \cdot 10^{-6} = 0.5pF$$

This is the out-of-plane gap closing (OPGC) transduction capacitance studied in last chapter, which shows the movement along z-axis. Doing a comparison between the maximum capacitance of the beam cantilever when the minimum separation between beams is $s = s_0/6$ and the comb capacitance. We see that the capacitance generated in the comb structure is lower.

$$C_{beam_{max}} = \frac{\varepsilon A}{s} = 6 \cdot \varepsilon \cdot \frac{A}{s_0} \tag{3.30}$$

$$C_{beam_{max}} = 6 \cdot 8.85 \cdot 10^{-12} \cdot \frac{6.4 \cdot 10^{-7}}{8 \cdot 10^{-6}}$$

$$C_{beam_{max}} = 4.2pF$$

To obtain the same capacitance, it is necessary to determine the width of the finger when both capacitances are the same $C_{comb_{max}} = C_{beam_{max}}$.

$$6 \cdot \varepsilon \cdot \frac{A}{s_0} = 0.4 \cdot \left(\frac{w}{w_f}\right)^2 \cdot \varepsilon \cdot t_f \tag{3.31}$$

$$6 \cdot \varepsilon \cdot \frac{w^2}{s_0} = 0.4 \cdot \left(\frac{w}{w_f}\right)^2 \cdot \varepsilon \cdot t_f \tag{3.32}$$

$$w_f = 0.26 \cdot \sqrt{s_0 \cdot t_f} = 3.43\ \mu m \tag{3.33}$$

So, the number of gaps required is calculated using the equation 3.26

$$N_g = \frac{0.8 \cdot 10^{-3}}{3.43 \cdot 10^{-6}} = 233$$

3.4.1. DC voltage applied in comb cantilever

The figure 46 shows a damped oscillatory movement which is almost identical to beam cantilever response. The limits in y-axis shows negative values because the current structure has the ability to move with non-stop limit as beam cantilever has. It is possible to notice a decrement in cantilever voltage due to the quick variation in capacitance and comparing to the beam structure, it shows less voltage.

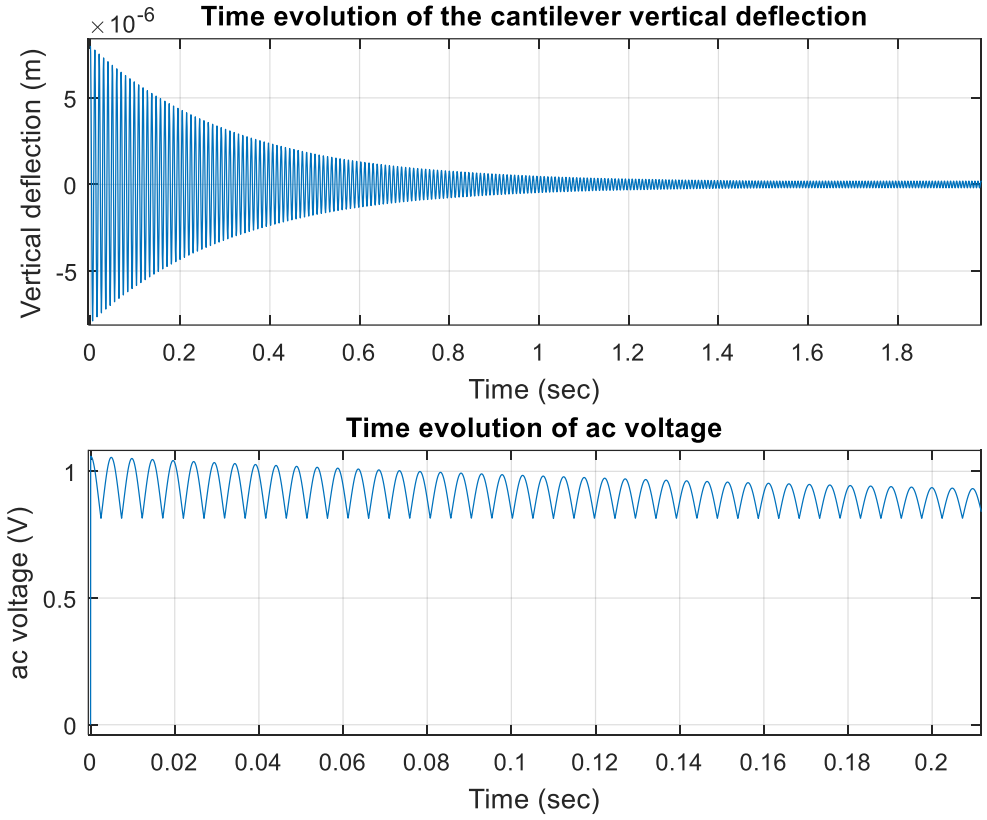

Figure 45: Comb cantilever response at DC voltage

In order to obtain positive values in vertical deflection, the following approach was analyzed.

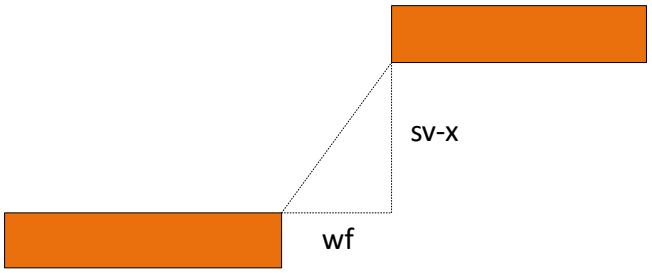

Figure 46: Difference in comb cantilever height structure

The height difference is set by the hypotenuse of the triangle between w_f and $s_v - x$, where s_v is a new design parameter introduced. The value of s_v is set initially to two times the thickness of the finger.

The figure below shows the cantilever response at DC input voltage, its maximum height in the damped oscillatory signal is $5.671 \cdot 10^{-8}\, m$ which is lower comparing to the previous model, but it shows a positive height only. Moreover, the cantilever voltage tagged as ac voltage shows a consistent variation comparing to the previous model, and its variation is almost the same as the open circuit voltage used in the input signal.

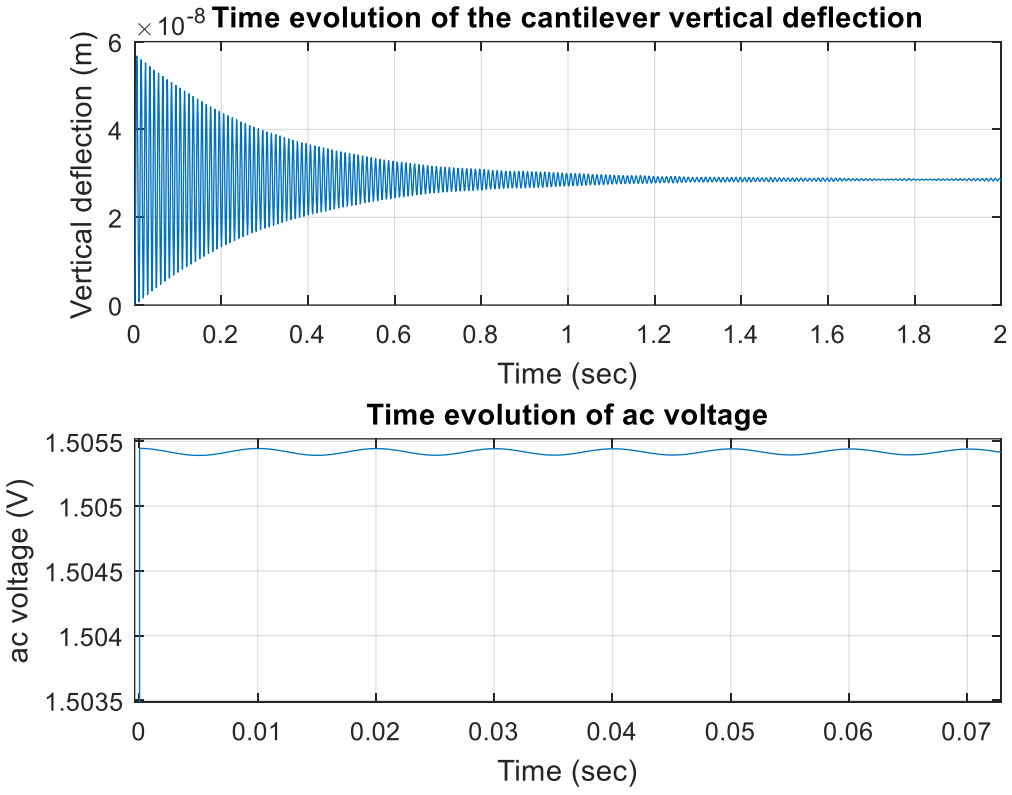

Figure 47: Comb cantilever vibration response using triangle approach

3.4.2. AC voltage applied to comb cantilever

A sinusoidal input signal was used to obtain a similar response as the beam structure. In the figure 48 the signal response is stabilized after 1.2 seconds, so comparing to the beam structure the responses are similar, and they show a typical spring mass system response. The cantilever output voltage shows almost the maximum voltage is stored in the comb capacitor cantilever, so the difference between the open circuit voltage and the current maximum voltage is $1.537463 - 1.505 = 0.032463\ V$.

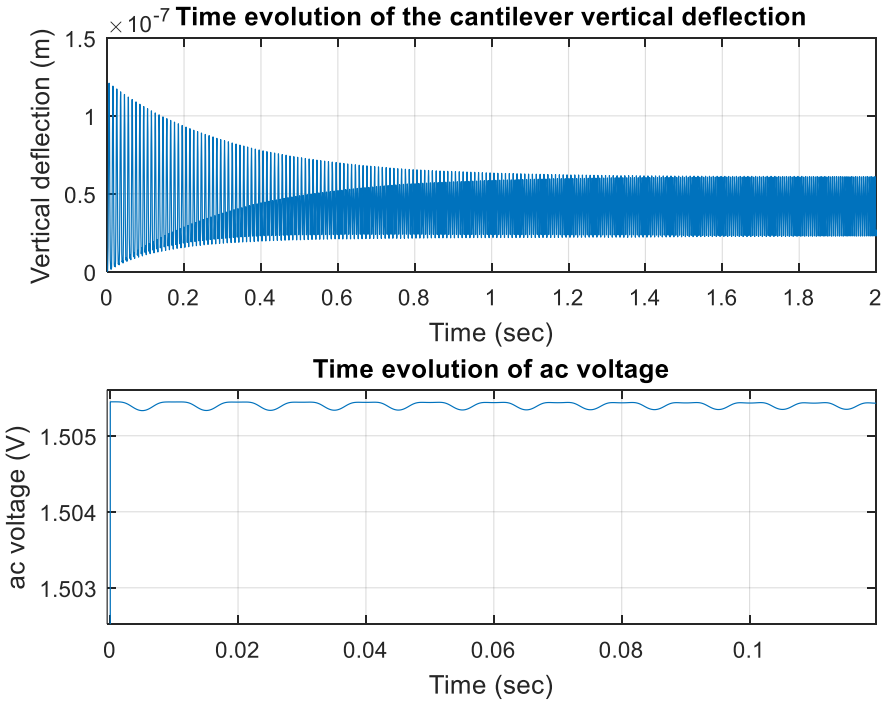

Figure 48: Comb cantilever sinusoidal response using triangle approach

Despite, the maximum voltage transferred to the comb capacitor the sound pressure level obtained is lower comparing to the beam structure. So, the sound power would be even less when the distance increases.

The Figure 49 shows that the minimum sound pressure level is produced at 0.15 cm from the source. As the c.

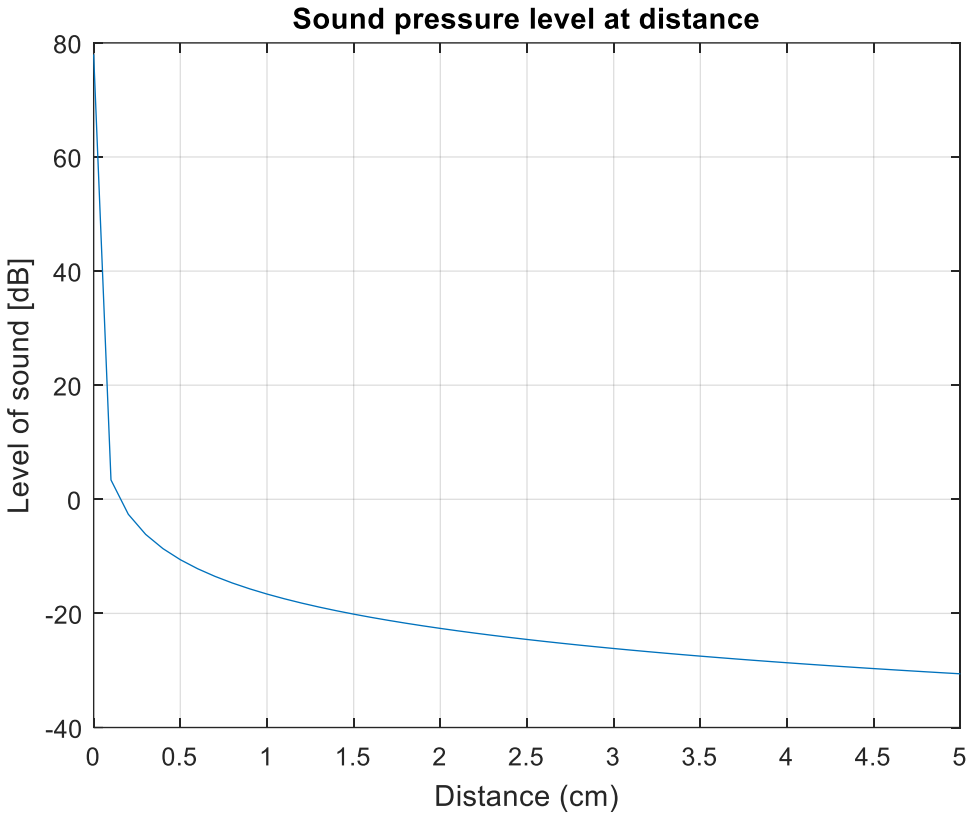

Figure 49: Sound pressure level from 0 to 5 cm in comb cantilever input sinusoidal signal using triangle approach

3.5. Patch antenna as cantilever

A rectangular patch antenna that can perform as a cantilever is proposed. Using air as the dielectric in the antenna substrate, the receiver antenna was designed to work at 1 GHz. The table 7 shows the dimension and the characteristic parameters of the antenna.

Parameters	
Frequency	1 GHz
Permittivity ε_r	1
Substrate height	1 mm
Thickness	35µm
Width	15 cm
Length	14.86 cm
Effective Permittivity $\varepsilon_{r_{eff}}$	1

Delta Length	0.7 mm
Effective Length	15 cm
Ground Plane Length	5.5 cm
Ground Plane Width	7.1 cm
Directivity	8.6 (9.3 dB)
Young modulus (copper)	119 GPa
Density (copper)	8960 Kg/m^3

Table 7: Receiver antenna parameters and dimensions (air substrate)

The maximum voltage is located in the edges of the patch antenna in T10 transmission model mode. So, the figure 51 shows the antenna structure, where a dielectric pivot is placed in the half of the antenna's length, it separates the patch and the ground plane to fix the movement just in its edges. Besides, as a parameter design the ground plane is fixed to limit the damped oscillatory movement in the structure.

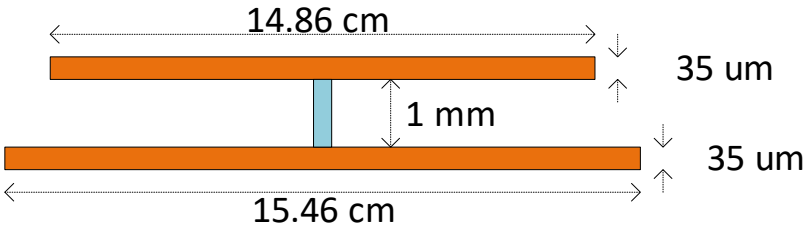

Figure 50: Receiver antenna structure air substrate

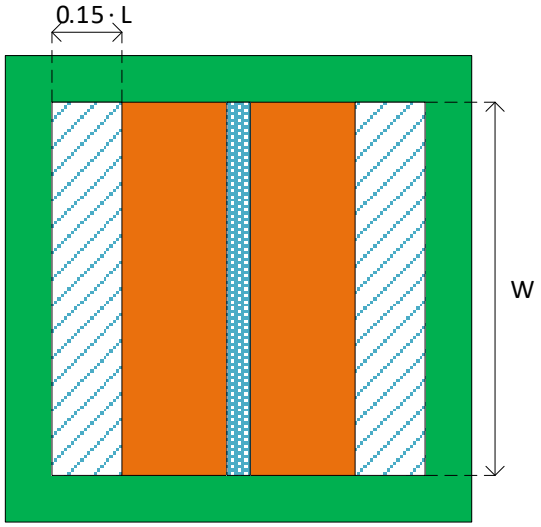

Figure 51: Top view of the antenna structure with air substrate

Additionally, the effective voltage in the antenna due to the cosenoidal distribution limit the length of both cantilevers. So, the effective length of the cantilever is set to $0.3 \cdot L/2$ as a design parameter. The figure 52 shows the effective area of the cantilever. It can be calculated as

$$A_{ee} = W \cdot 0.15 \cdot L = 0.15 \cdot 0.1486 \cdot 0.15 = 3.3\, mm^2 \tag{3.34}$$

The spring constant is 0.06 N/m, it is strongly dependent on the physical dimensions of the antenna.

3.5.1. DC voltage applied in the patch antenna

Considering, the open circuit voltage obtained at different distances which is shown in the figure 36, it is possible to simulate the antenna response stablishing an open circuit voltage of 1.537463 V. This voltage was obtained graphically from the figure 36 at a distance of separation between antennas of 4.51 m. The figure 53 shows the response at the continuous voltage applied to the patch antenna; the vibration of the patch antenna as a cantilever shows a damped oscillatory movement where at the end of the response it is getting the rest. The cantilever voltage in the structure is getting constant due to the antenna is working as a variable capacitance itself.

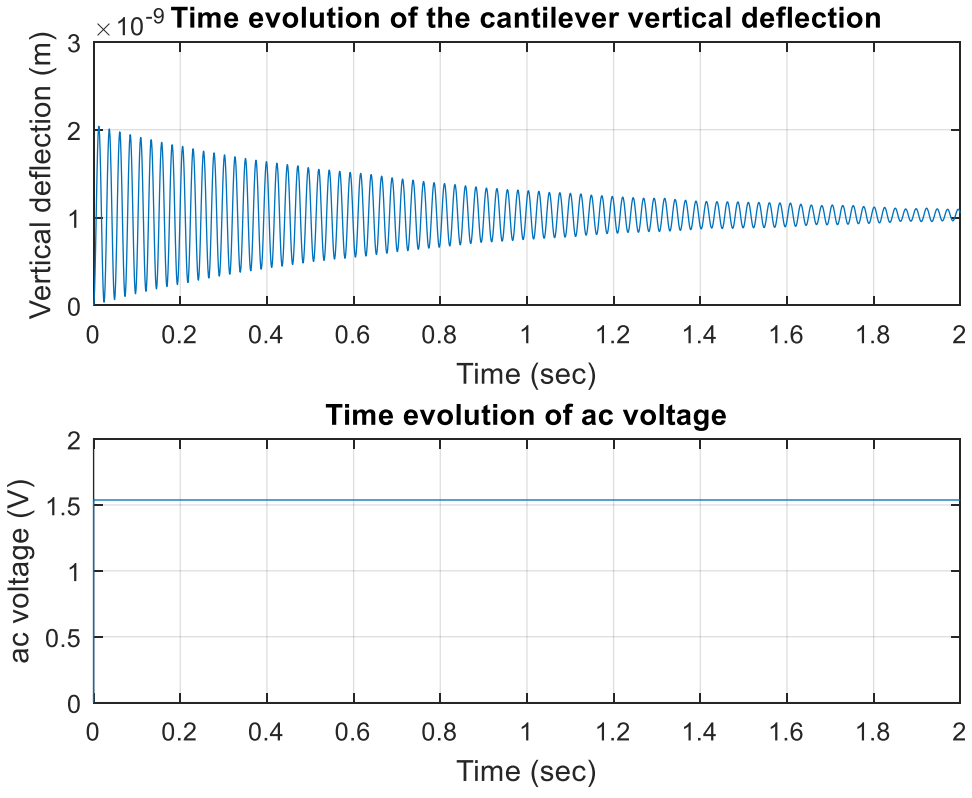

Figure 52: Rectangular patch antenna as cantilever response at 4.51 m of separation distance

3.5.2. Amplitude modulated signal applied to the patch antenna

The characteristic frequency of the cantilever was calculated using the MATLAB script developed, so taking into account the effective mass and the spring constant, the frequency obtained is 41.37 Hz. It is used as the modulating frequency in the simulation. In Figure 53 the response to an amplitude modulated signal is shown, it was simulated using an open circuit voltage of 1.537463 V. This voltage was obtained graphically from the figure 36 at a distance of separation between antennas of 4.51 m. It shows that a sinusoidal response which is increasing up to reach the its maximum amplitude after 1.8 seconds. The amplitude of the vertical displacement after 1.8 seconds is approximately $7.4 \cdot 10^{-8}\ m$ and its period showed in the figure 54 is 0.02 seconds which is equal to the modulating frequency.

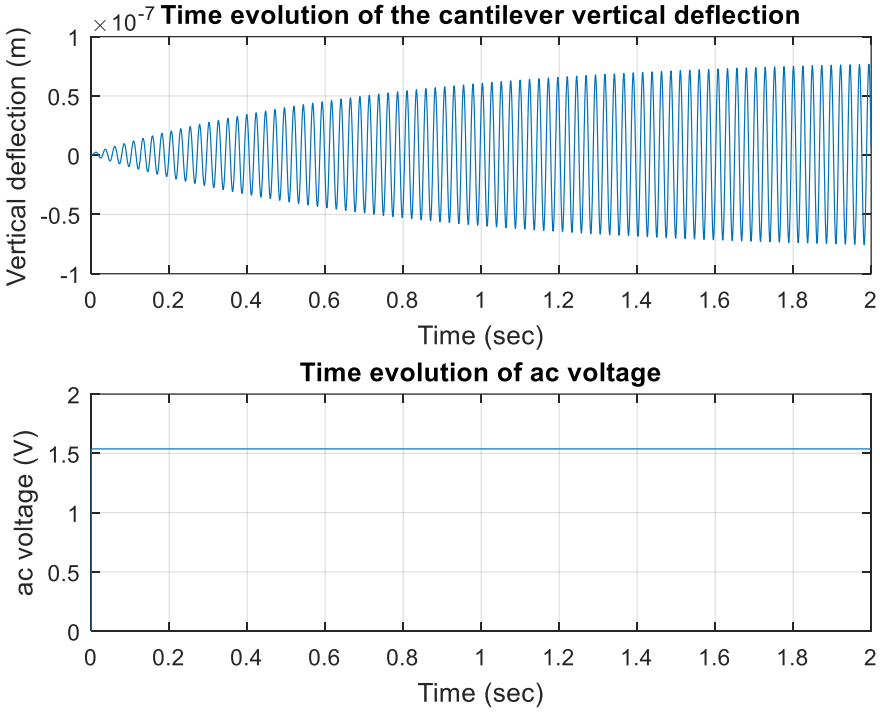

Figure 53: Amplitude modulated response of the rectangular patch antenna at 4.51 m of separation distance

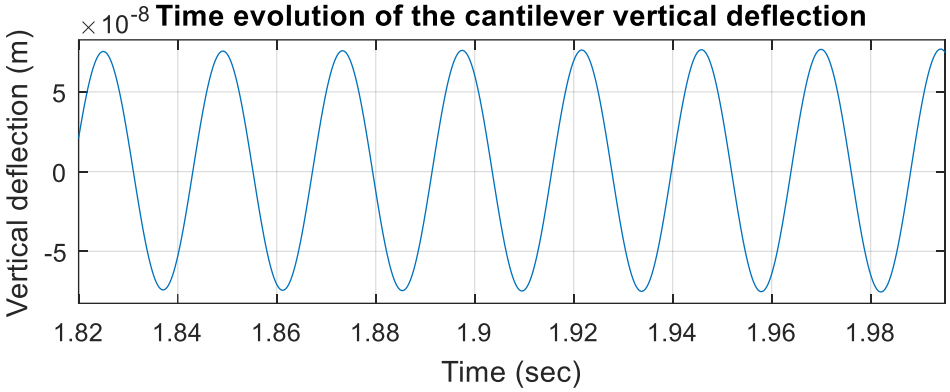

Figure 54: Amplitude modulated period of patch antenna at 4.51 m of separation distance

3.5.3. Sound pressure level produced in the patch antenna

Using the equations 3.22, 3.23 and 3.24, it was possible to determine the sound pressure level at different distances, from the vibration source (the patch cantilever), starting from 0 to 5 centimeters. It was simulated using an open circuit voltage of 1.537463 V. This voltage was obtained graphically from the figure 36 at a distance of separation between antennas of 4.51 m.

$$v_{rms} = 2\pi \cdot f_{cantilever} \cdot A = 2\pi \cdot 41.37 \cdot 7.4 \cdot 10^{-8} = 1.99 \cdot 10^{-5}\ m/s$$

$$P_{rms} = \rho_{air} \cdot c_{air} \cdot v_{rms} = 1.225 \cdot 343 \cdot 1.99 \cdot 10^{-5} = 8.36 \cdot 10^{-3}\ Pa$$

$$SPL\ (dB) = 20 \log\left(\frac{8.36 \cdot 10^{-3}}{2 \cdot 10^{-5}}\right) = 52.42\ dB$$

The amplitude A used in the equation to calculate v_{rms} is the same as in the previous section. As we can see the sound pressure level obtained at the source is higher than the minimum audible stablished as the reference.

The calculus of the sound pressure level along the distance is shown in the figure 55; the output signal shows that the pressure is decreasing asymptotically as the distance increase but it continues being higher than the minimum. It happens because the contribution of the effective area increases proportionally the Rayleigh length which is described in section 3.3.6. Consequently, the pressure remains high despite of the increase in distance.

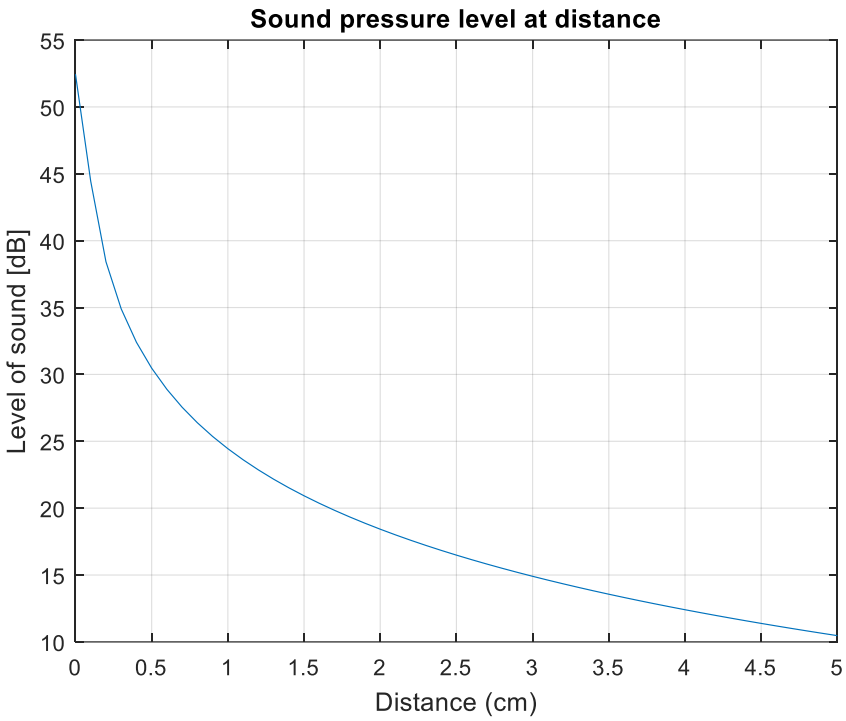

Figure 55: Sound pressure level from 0 to 5 cm in patch antenna using amplitude modulated signal at 4.51 m of separation distance between antennas

4. Measurements

The practical implementation of the system is shown in the figure 54 where the instrumentation and elements were used to perform AM modulation.

- The rectangular microstrip patch antenna previously designed in chapter 3 was fabricated using ROGERS 3010 as its PCB material.
- The signal generator HP 8647A which can work in the range of frequencies from 250 KHz to 1000 MHz; it can modulate the input signal in amplitude or in frequency, but the internal available modulating frequencies are limited to 400 Hz and 1 KHz. Despite of this limitations, the equipment can accept the stimulation of an external modulating signal.
- Due to the limitation of the HP generator. It was necessary the use of an additional signal generator HAMEG HM8131-2 to generate the modulating signal. It can generate signals up to 15 MHz
- The RF power amplifier RF101000-10 RFPA was used to amplify the signal produced by the signal generators. It adds 40 dB of power to the input signal. At the end, the output signal generated by the amplifier is transmitted to the patch antenna.
- In the other side, a dipole cantilever was used as the receiver antenna and the microelectromechanical device. To displace horizontally the cantilevers, a micrometric screw was used and it helped us to obtain the required gaps. Due to the required gaps are in micro scale, a microscope was used to zoom in the area of separation.
- To measure the vertical displacement produced by the cantilever vibrations, the Position Sensitive Detector PSD New Focus 2930 and a laser were used. The Position Sensitive detector consist of a p-n junction photodiode which can measure the photocurrents generated by the incoming red-light. The light produced by the laser has 1.2 mW of red-light power and it has a wavelength of 635 nm.

The output signal obtained by the Position Sensitive Detector is sent to the Tektronix MDO3024 oscilloscope. It displays the voltage variation measured in the photodiode.

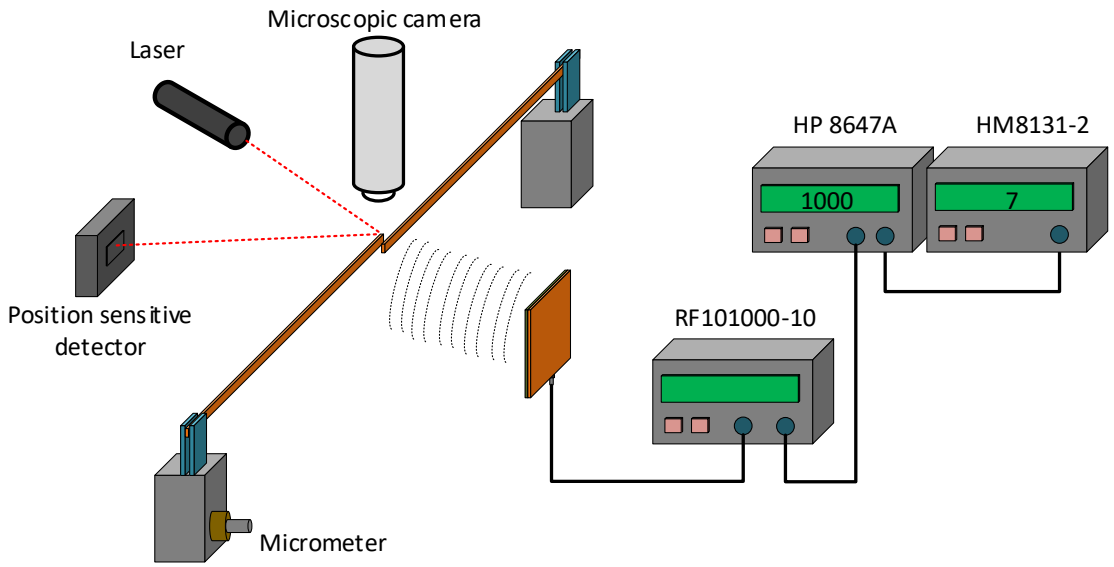

Figure 56: Practical implementation of the system

4.1. Antenna measurements

Regarding to the antenna measurements, the scattering parameters S11, S22 and S12 was obtained using the E5061B ENA Agilent network analyzer. To obtain the practical operational frequency of the antenna, a frequency sweep was done starting from 800 MHz to 1.1 GHz. Thereby, the operational frequency is located at 918.31 MHz; despite of the analysis and design of the antenna did in chapter 3 where the dimensions were calculated. In practice, the frequency of operation is influenced due to material characteristic variations.

The S11 parameter is shown in the figure 57. The minimum reflection coefficient of the transmitter antenna is set at 918 MHz where the value obtained is -6.75 dB.

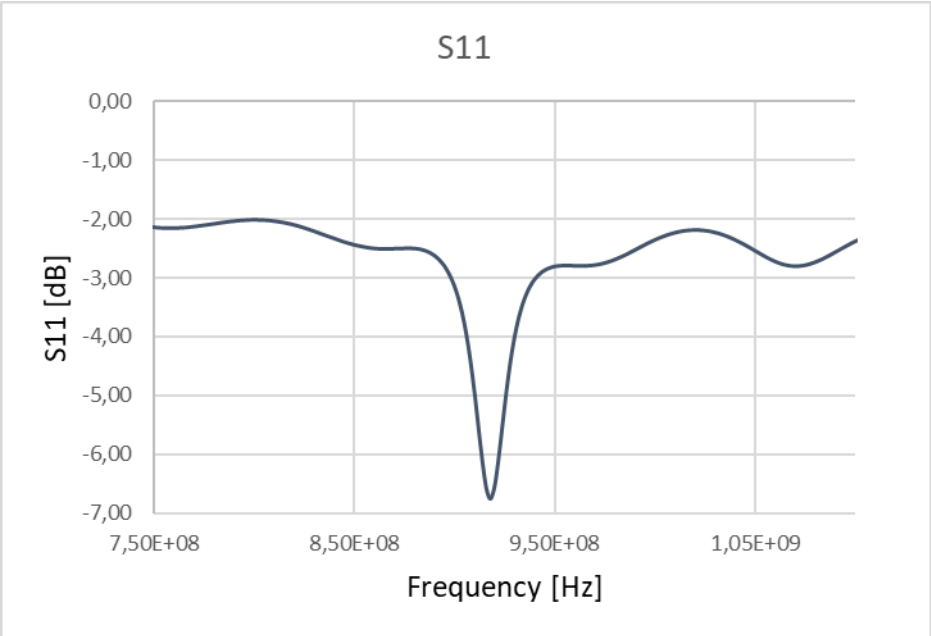

Figure 57: S11 parameter in transmitter antenna

It means that the reflection coefficient in non-logarithmic scale is

$$S = 10^{-\frac{6.75}{10}} = 0.2113 \tag{4.1}$$

So, the reflection mismatch efficiency is calculated using the equation 3.1 as

$$e_r = 1 - S^2 = 1 - (0.2113)^2 = 0.9553$$

The available power in the antenna is set to 44 dBm (25.12 W) because the RF generator, the accepted power by the antenna is calculated using the equation 3.2

$$W_a = W_s \cdot e_r = 25.12 \cdot 0.9553 = \ 23.99\ W$$

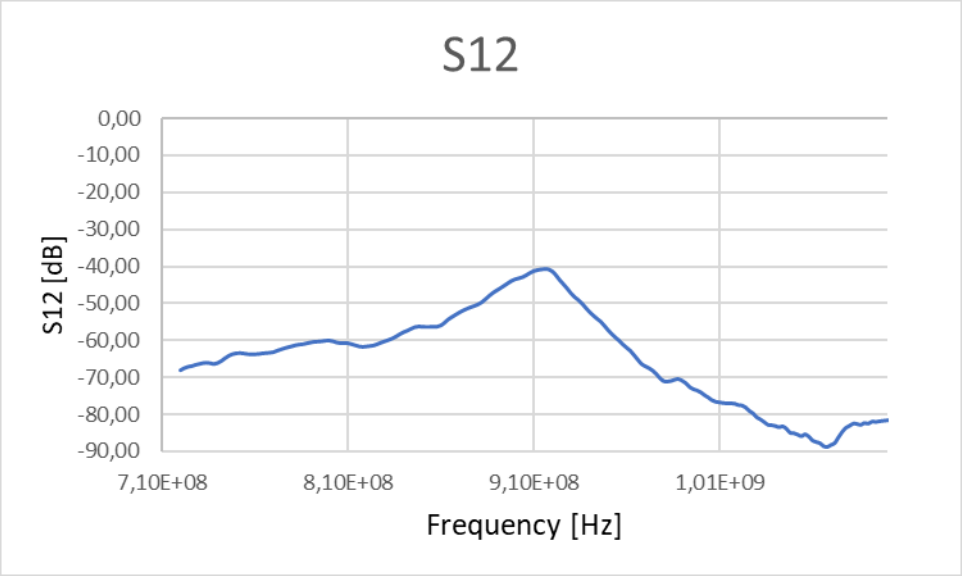

Figure 58: S12 parameter in transmitter antenna

From the S12 parameter in the figure 58 it is possible to determine that the radiated power by the antenna is calculated using the equation 3.3

$$W_r = W_a \cdot S_{12} = 23.99 \cdot 10^{-4} = 2.3\ mW$$

The antenna impedance obtained in the Agilent E5061B network analyzer is shown in the figure 59, it is $34.09 - j \cdot 39.73\ \Omega$. Due to the impedance is negative in the imaginary axis, it represents capacitive behavior compared to the reference impedance of 50 ohms.

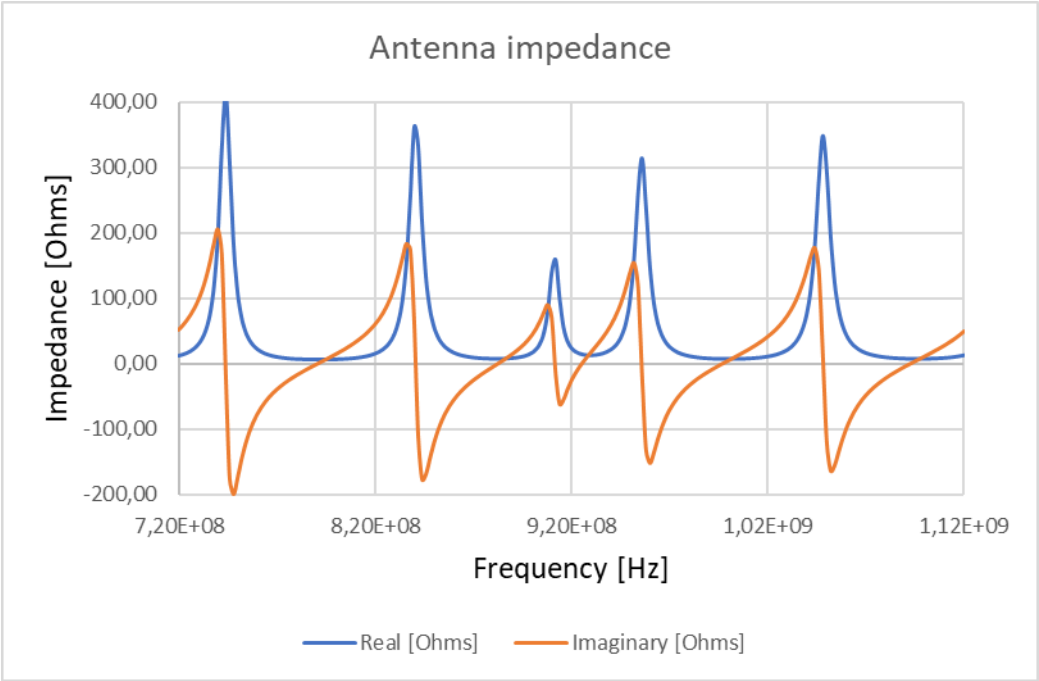

Figure 59: Antenna impedance in transmitter antenna

4.2. Dipole Cantilever measurements

The dipole cantilever used as the microelectromechanical receiver antenna was designed in previous projects to operate at 920 MHz, its dimensions are fitted not only to work as antenna but also to work in its ends as a microelectromechanical element.

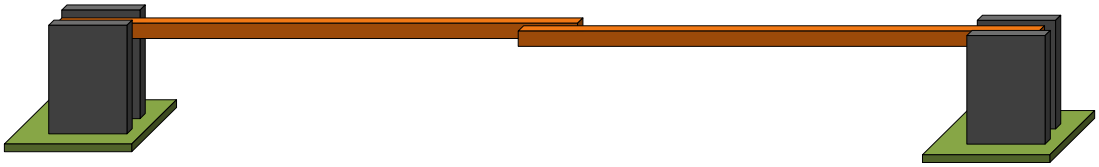

Figure 60: Microelectromechanical receiver antenna at 920 MHz

The dimensions of the cantilever used in laboratory are shown in figure 61, where the length of the dipole is about 17.5 cm, the width is 2 mm and the thickness is 0.1 mm.

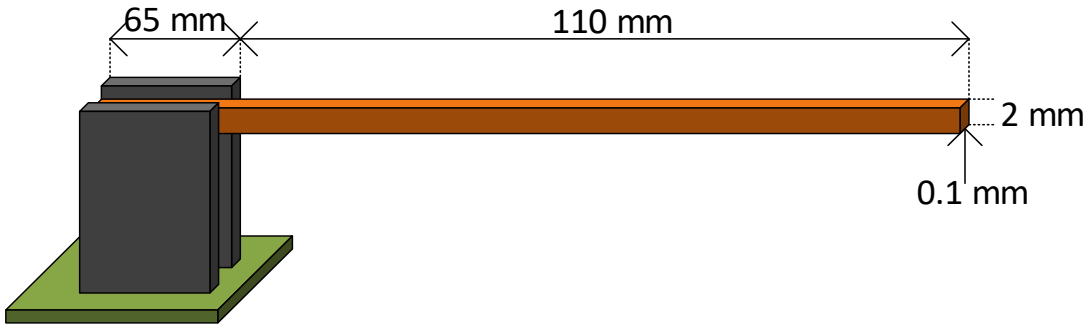

Figure 61: Cantilever dimensions used in laboratory

The figure 62 shows the overlapping length is set to 1 mm. It was moved along the horizonal plane until to reach the required gap.

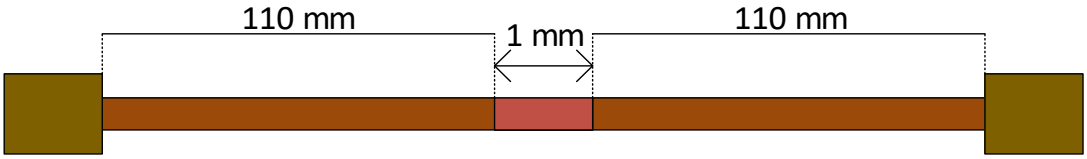

Figure 62: Cantilever overlapping width top view

To test the vibrations in the cantilever, a separation distance of 10 cm between the cantilever and the rectangular microstrip antenna was set.

4.2.1. Collapse voltage measurements

4.2.1.1. Case of 96 micrometers of gap

The initial test set a gap of 96.2 μm as it is shown in figure 63. The available power set in the test increases from 35 dBm to 45 dBm due to the contribution of the amplifier.

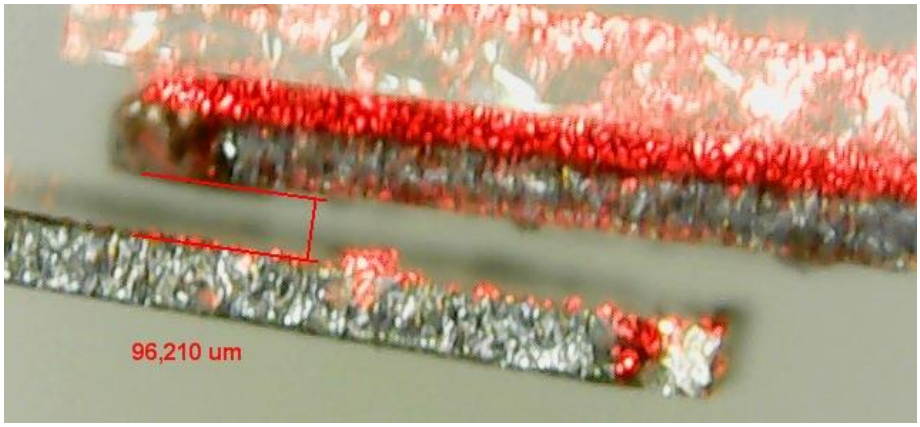

Figure 63: Gap of 96.2 um between cantilevers

In table 8, it is possible to determine the necessary power to collapse the cantilever at the given gap and the distance of separation of the transmitter. The maximum transmitting power accepted for the system at 10 cm of separation between antennas and the given gap is 42 dBm because in higher voltage the variation measured by the photodiode remains the same value of 75 mV. To obtain the displacement along the z axis due to the cantilever vibration, the following experimental equation was used

$$z = \left(\frac{2}{3}\right) \cdot L \cdot \tan\left(0.8 \cdot 10^{-3} \cdot \frac{V_{osc}}{2 \cdot 180 \cdot 10^{-3}}\right) \quad (4.2)$$

Where L is the length of the cantilever, V_{osc} is the variation voltage measured in the oscilloscope. In table 8 the displacement along z axis shows that the collapse of the structure starts from 42 dBm of available power because the current displacement of 122 micrometers is higher than the initial gap.

Available power dBm	Variation of voltage mV	Z – axis displacement [m]
35	10	1,63E-05
36	15	2,44E-05
37	18	2,93E-05
38	20	3,26E-05
39	20	3,26E-05
40	25	4,07E-05

41	28	4,56E-05
42	75	1,22E-04
43	75	1,22E-04
44	75	1,22E-04
45	75	1,22E-04

Table 8: Voltage measured by the photodetector at 96.2 um of gap

The figure 64 shows high slope response in the range of 41 to 42 dBm when the cantilever is close to collapse, it means that the photodiode is absorbing almost the totality of the reflected light of the laser.

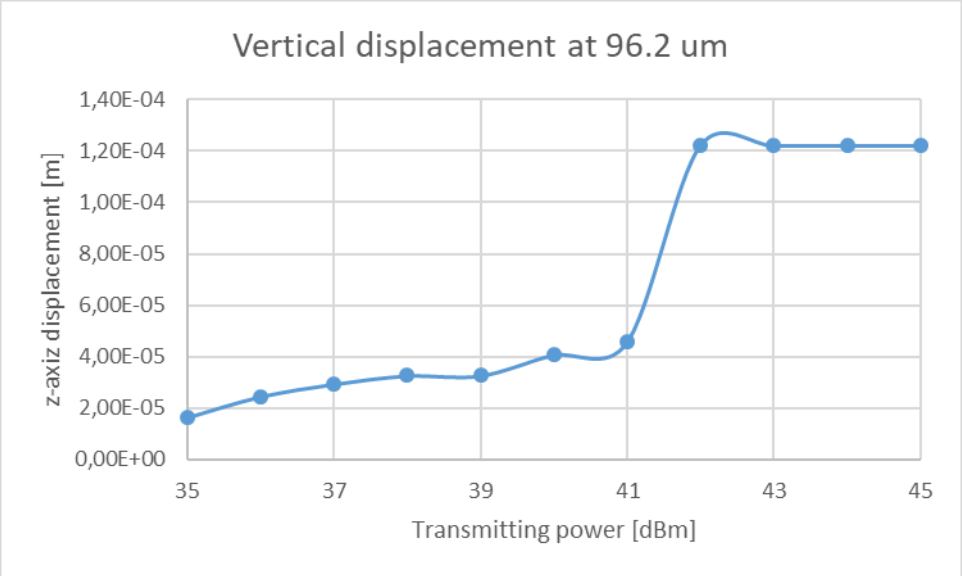

Figure 64: Vertical displacement at 96.2 um of gap

4.2.1.2. Case of 119 micrometers of gap

The figure 65 shows a gap of 119.3 μm. The available power set in the test increases from 35 dBm to 48 dBm. It varies from the previous case due to it is necessary a higher power to collapse the cantilevers.

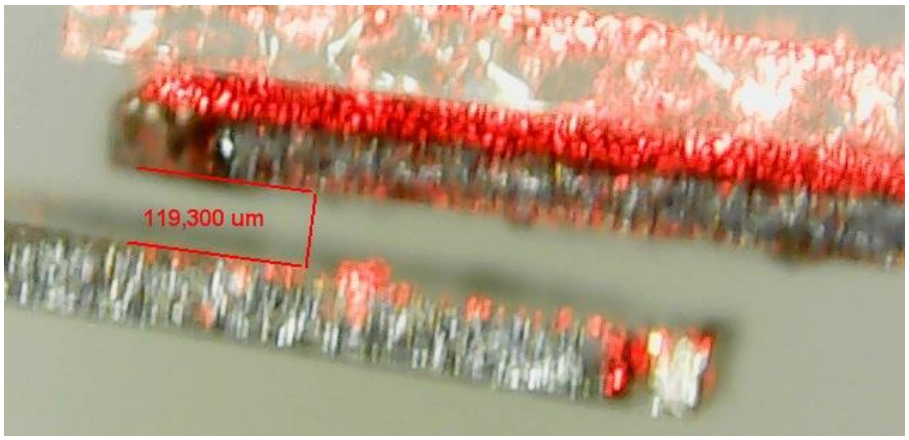

Figure 65: Gap of 119.3 um between cantilevers

Available power [dBm]	Variation of voltage [mV]	Z – axis displacement [m]
35	10	1,63E-05
36	16	2,61E-05
37	18	2,93E-05
38	25	4,07E-05
39	28	4,56E-05
40	40	6,52E-05
41	40	6,52E-05
42	45	7,33E-05
43	53	8,64E-05
44	67	1,09E-04
45	70	1,14E-04
46	70	1,14E-04
47	70	1,14E-04
48	70	1,14E-04

Table 9: Voltage measured by the photodetector at 119.3 um of gap

In table 9, it is possible to determine the necessary power to collapse the cantilever at the given gap and the distance of separation of the transmitter. The maximum transmitting power accepted for the system at 10 cm of separation between antennas and the given gap is 45 dBm because in higher voltage the variation measured by the photodiode remains the same value of 70 mV. The figure 66 shows an almost linear response along the transmitting power used, it means that the photodiode is absorbing less energy produced from the laser due to the increase in the gap.

Using the displacement equation 4.2 set in the previous section, it is possible to determine the collapse of the structure as a function of the voltage measured in the oscilloscope

In the table 9 third column, the displacement along z axis shows that the collapse of the structure starts from 45 dBm of available power because the displacement at this power is 122 micrometers which is almost the same as the initial gap.

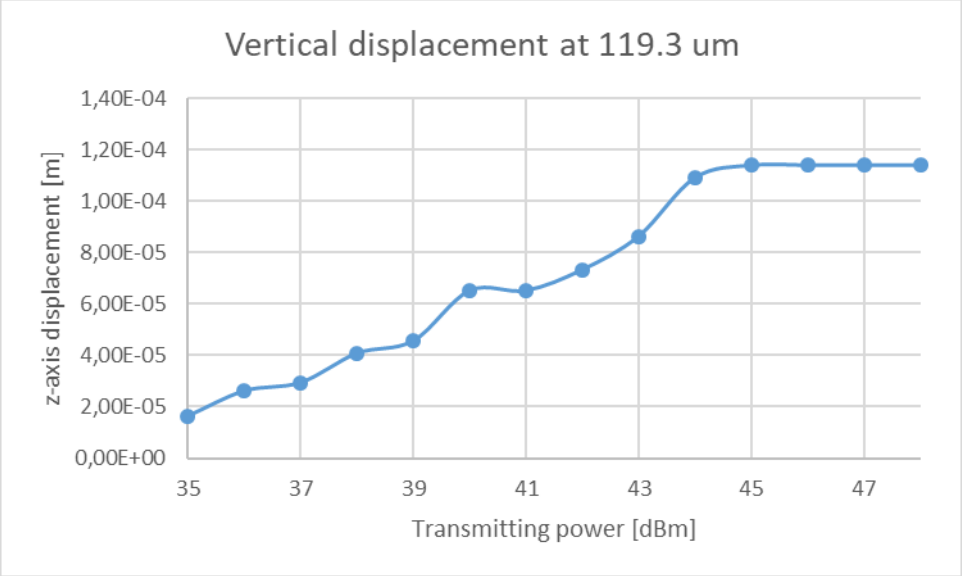

Figure 66: Vertical displacement at 119.3 um of gap

4.2.1.3. Case of 130 micrometers of gap

The figure 65 shows a gap of 130.775 µm. The available power set in the test increases from 35 dBm to 49 dBm. It varies from the previous case due to it is necessary a higher power to collapse the cantilevers.

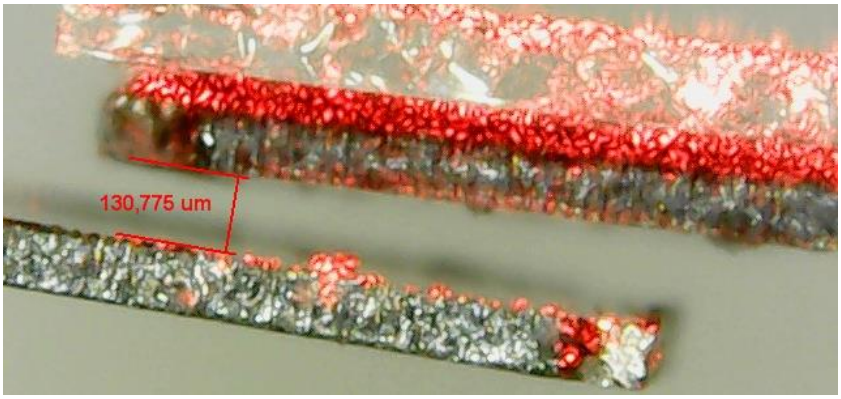

Figure 67: Gap of 130.775 um between cantilevers

Available power dBm	Variation of voltage mV	Z – axis displacement [m]
35	10	1,63E-05
36	12	1,96E-05
37	12	1,96E-05
38	15	2,44E-05
39	22	3,59E-05
40	25	4,07E-05
41	30	4,89E-05
42	35	5,70E-05
43	42	6,84E-05
44	50	8,15E-05
45	60	9,78E-05
46	60	9,78E-05
47	80	1,30E-04
48	80	1,30E-04
49	80	1,30E-04

Table 10: Voltage measured by the photodetector at 130.775 um of gap

In table 10, it is possible to determine the necessary power to collapse the cantilever at the given gap and the distance of separation of the transmitter. The maximum transmitting power accepted for the system at 10 cm of separation between antennas and the given gap is 7 dBm because in higher voltage the variation measured by the photodiode remains the same value of 80 mV.

Using the displacement equation 4.2 set in the previous section, it is possible to determine the collapse of the structure as a function of the voltage measured in the oscilloscope as the table 10 third column shows.

The figure 68 shows an almost linear response along the transmitting power used, it means that the photodiode is absorbing energy proportionally from the laser.

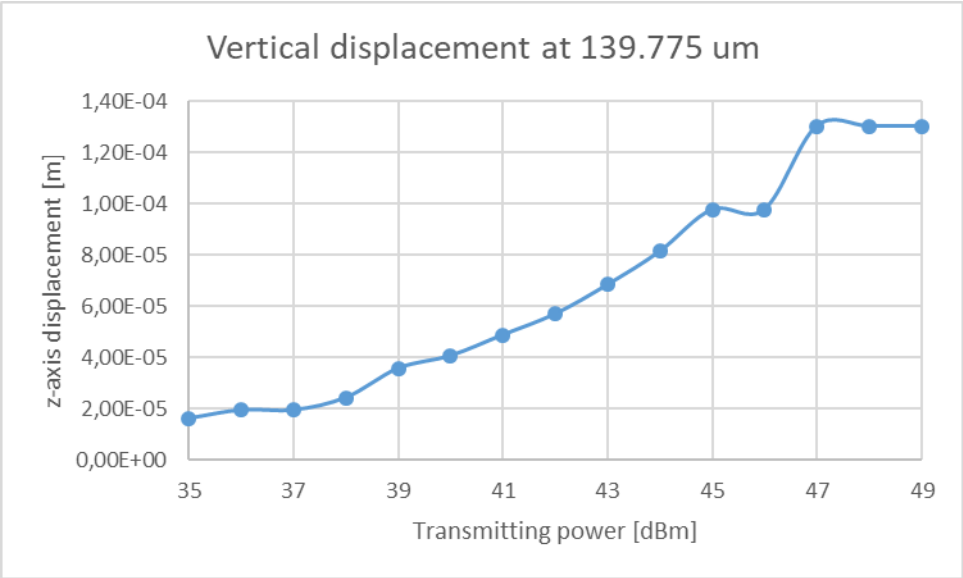

Figure 68: Vertical displacement at 130.775 um of gap

The figure 69 shows after transmitting 7 dBm of RF power the voltage measured by the PSD drops up to the origin in x axis, it is the normal behavior of the system when the cantilever is excited by a continuous signal.

After some time, the transmitting power stops, the cantilever response shows the harmonical oscillatory characteristic response studied in chapter 3 when a DC voltage is applied to the structure. It is good to mention that RF signals in microelectromechanical systems are taken as continuous in time signals; due to the physical structure, it is not possible get vibrations at ultra-high frequencies.

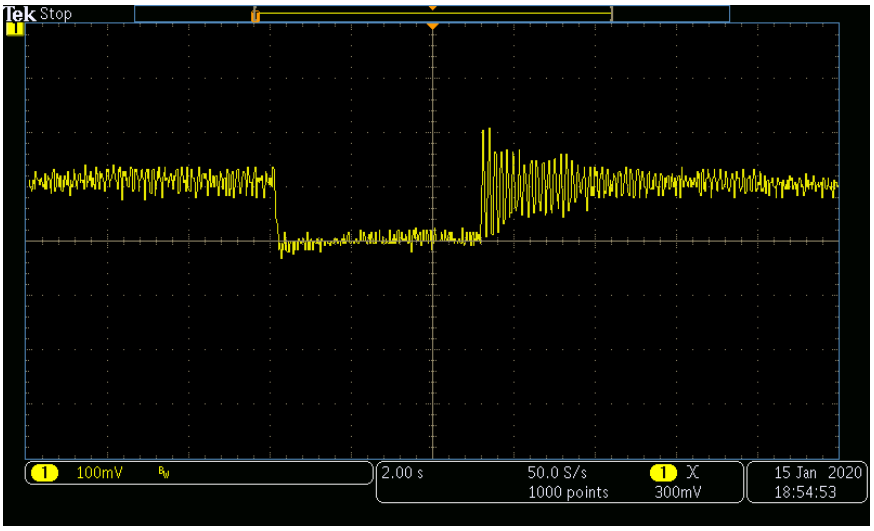

Figure 69: Collapsing voltage in cantilever at 130.775 um

4.2.2. Amplitude modulated measurements

The figure 70 shows the response due to amplitude modulated signal transmitted by the patch antenna at 10 cm of separation distance. It was used an index modulation percentage of 100% to obtain the maximum amplitude of the modulating signal, so based on the equations described in theory section both amplitudes have to be equal and they were set to 4 dBm (44 dBm after RF amplifier), because it was a limitation of the external input power signal in the HP 8647A signal generator.

The HP 8647A signal generator was set to operate to 918 MHz, it is the resonance frequency of the antenna, to produce the RF sinusoidal signal.

The HM8131-2 HAMEG signal generator was set to operate at 7 Hz, to produce the modulating signal. Due to the dimensions of the cantilever used in laboratory, the characteristic frequency is grouped in the extremely low frequencies range.

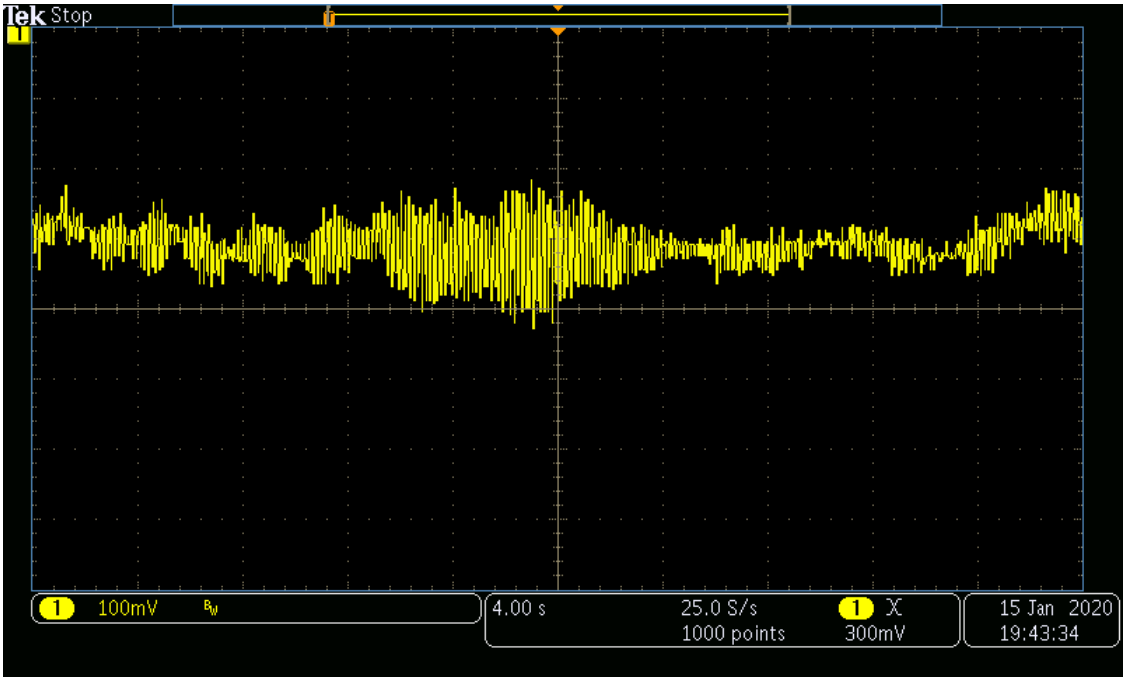

Figure 70: Amplitude modulated response in the cantilever from 6 to 8 Hz

The frequency sweep was, synchronized with the oscilloscope sweep, it was programmed in the HM8131-2 HAMEG signal generator, so that the mechanical frequency response of the cantilever could be visualized in the oscilloscope. The frequency sweep was set from 6 Hz to 8 Hz and it is shown in the figure 70. The response shows that the greater variations measured by the PSD are located around 7 Hz; So, in lower and higher frequencies the voltage variations shows less contribution.

The figure 71 shows the operating frequency of the receiver antenna is set to 7 Hz where the maximum variation voltage obtained from the PSD is located.

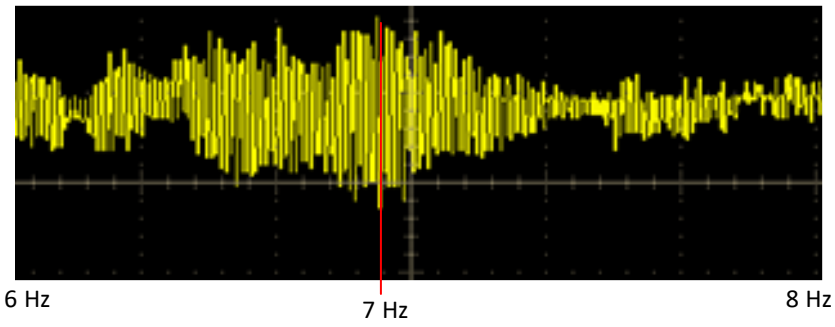

Figure 71: Amplitude modulating response in the cantilever from 6 to 8 MHz

From the figure 72, it is possible to determine the value of the maximum variation voltage that can help us to calculate the maximum vertical displacement in the cantilevers structure. Its value is obtained based on the voltage per division reference in the oscilloscope, it is set to 100 mV per division. Each division has 10 subdivisions and it helps to obtain graphically the maximum amplitude in the response.

Measuring from the blue line which is located as the x-axis reference, the maximum amplitude is enclosed to 5.5 subdivisions. So, the maximum voltage amplitude is

$$V_{osc} = 100\ mV \cdot \frac{5.5}{10} = 55\ mV \tag{4.3}$$

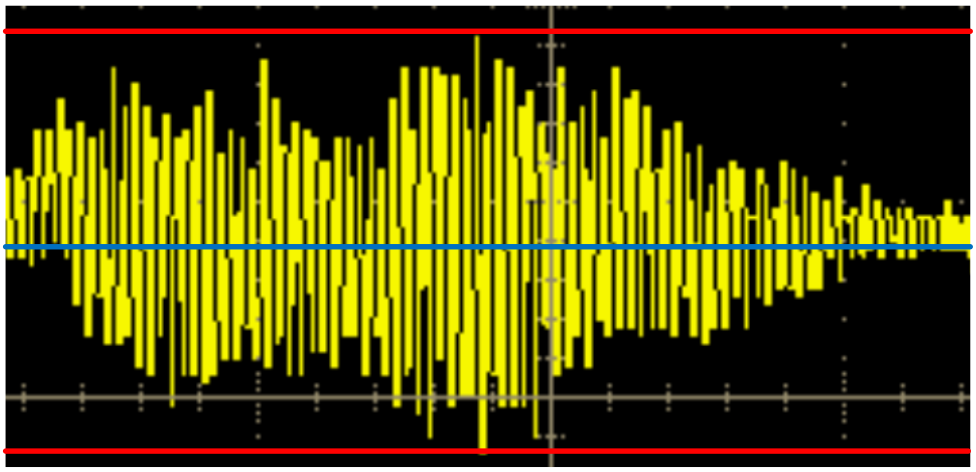

Figure 72: Amplitude modulated response at 918 MHz (carrier) and 7 Hz (modulator)

To calculate the vertical displacement of the cantilever the equation 4.2 was used. Where the length of the cantilever is 11 cm and the voltage measured in the oscilloscope is shown in the equation 4.3

$$z = \left(\frac{2}{3}\right) \cdot 0.11 \cdot \tan\left(0.8 \cdot 10^{-3} \cdot \frac{55 \cdot 10^{-3}}{2 \cdot 180 \cdot 10^{-3}}\right)$$

$$z = 1.56 \cdot 10^{-7}\ m$$

Using the equations 3.22, 3.23 and 3.24 described in the previous chapter, it was possible to determine the sound pressure level at the source as

$$v_{rms} = 2\pi \cdot f_{cantilever} \cdot A = 2\pi \cdot 7 \cdot 1.56 \cdot 10^{-7} = 6.86 \cdot 10^{-6}\ m/s$$

$$P_{rms} = \rho_{air} \cdot c_{air} \cdot v_{rms} = 1.225 \cdot 343 \cdot 6.86 \cdot 10^{-6} = 2.88 \cdot 10^{-3}\ Pa$$

$$SPL\ (dB) = 20 \log\left(\frac{2.88 \cdot 10^{-3}}{2 \cdot 10^{-5}}\right) = 43.17\ dB$$

The figure 73 shows the sound pressure level along a range of distances from 0 to 5 centimeters. It is possible to determine that it decreases asymptotically as the distance increase, but taking into account that the minimum sound pressure value as the reference of 0 dB, the sound pressure level produced by the cantilever is higher than the minimum established up to 0.25 centimeters of separation distance with the source, approximately.

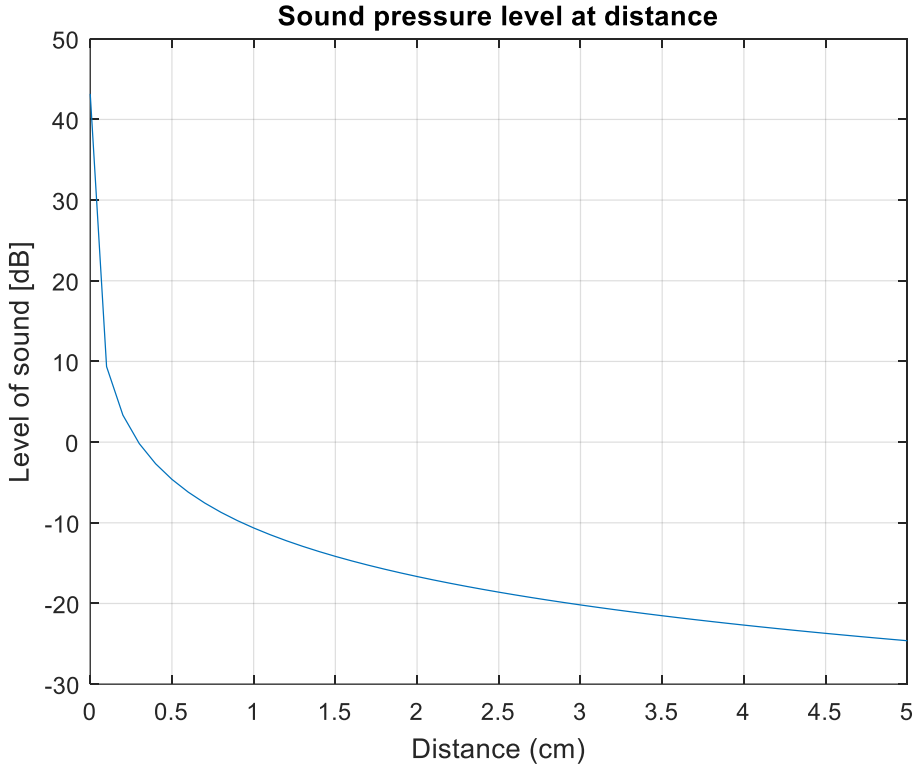

Figure 73: Sound pressure level from 0 to 5 cm in the experimental cantilever at 10 cm of separation distance

Regarding to the audible sound, the human ear cannot detect sound frequencies less than 20 Hz so, any sound below this frequency will be inaudible sound for humans. Therefore, from the experimental setup it was not possible to listen any sound because the frequency of vibration of the cantilever is below to the audible, although the sound pressure level up to 0.2 cm is higher than the minimum reference.

5. Conclusions

In summary, the main conclusions of this work are the following:

- It has been established the State of Art of the project and the bibliographic data collection.
- It has been designed a rectangular microstrip patch antenna. The design was done based on the characteristic values of the equipment available in laboratory like the gain of the RF Power amplifier RF 101000-10 RFPA which has a 40-dB gain. The frequency of operation was stablished to operate at 1 GHz due to the limitation of the HP 8647A signal generator. To obtain some of the characteristic design parameters of the antenna, a MATLAB script was developed. This script returns the values of the length and the width, the directivity of the antenna. In Feko antenna simulator, the values calculated by the MATLAB script were introduced and configured to simulate the antenna. The reflection coefficient has its minimum at 1 GHz and its value is set to -17.8593 dB, it means that efficiency mismatch allows the transmission of the 92% of the power available. The radiation efficiency takes the radiation resistance equal to 50 ohms as a parameter design, and from the simulation the real part of input impedance is 62, so the radiation efficiency is 80%. The power radiated by the antenna was calculated as the product of the efficiencies by the available power. Consequently, the 76% of the available power is radiated.
- The mathematical models that perform the functionality of the whole system was developed using MATLAB. It was necessary to separate the code in modules to have a better comprehension of the system. One of the modules, calculates the antenna parameters, the other module solves the characteristic differential equation of the cantilever model studied using Runge Kutta of 4^{th} order as a numerical method. The dimensions of the cantilever, were scaled down from the initial values took from previous projects to reduce the its dimensions to fit them to musical notes as audible frequencies.
- It has been done an analysis in DC of the structures and it was possible to see that they have damped oscillatory movements which is the characteristically response of the spring mass system studied.
- The AC analysis of the structures were done; the clamped free beam shows a vertical displacement of 0.2 μm and it is getting stable after 1.2 seconds . The

comb structure shows a vertical displacement of 70 nm and is getting stable after 1.2 seconds. The vertical displacement figures show that the stability of the system takes time.

- It has been studied the cantilever response at amplitude modulated signal. In the beam structure it was possible to see that the system has the ability to demodulate the input signal moving at the same time both beam cantilevers, the output signal obtained shows the vertical displacement of 0.7 μm. In the patch antenna as a cantilever structure the vertical displacement obtained is 74 nm. The patch antenna was design to operate at 1 GHz using air as the substrate and stablishing a substrate height of 1 mm. Due to the dimensions of the antenna designed the structure has bigger area than the other structures.
- It has been calculated the sound pressure level in the system. The sound pressure level in the beam cantilever structure is 77.95 dB but it decreases asymptotically when the distance increase. This is because, the effective area $0.64\ \mu m^2$ of the cantilever can affect the sound propagation because the pressure decreases quickly and overpass the minimum audible. The sound pressure level in the patch antenna structure was analyzed. Its value is 52.42 dB, the response from 0 to 5 cm decrease almost exponentially because the effective area is bigger than the beam cantilever.
- It has been measured the characteristic response of the cantilever due to an amplitude modulated signal. In the laboratory, it was possible to use the HP 8647A and HAMEG HM8131-2 signal generators to generate the amplitude modulated signal. This signal was transmitted to the RF amplifier to add 40 dB of gain and transmit it to the rectangular patch antenna. In the oscilloscope, it was possible to see the voltage measured by the Position Sensitive Detector, it shows the modulating signal transmitted. The vertical displacement was measured setting a separation distances between antennas of 10 cm and using a transmission power of 44 dBm. At these conditions, the sound pressure level produced by the cantilever vibration is higher than the minimum audible up to 0.25 cm, but as the natural frequency of the cantilever is 7 Hz, it was not possible to listen any sound from it.

Bibliography

[1] Noor Hidayah Mohd Yunus, Jahariah Sampe, Jumril Yunas and Alipah Pawi, "MEMS Based RF Energy Harvester for Battery-Less Remote Control," Universiti Kebangsaan, Malaysia, 2017.

[2] Adamu Murtala Zungeru, Li-Minn Ang, SRS. Prabaharan, Kah Phooi Seng, "Radio Frequency Energy Harvesting and Management for Wireless Sensor Networks," The University of Nottingham, Malaysia, 2012.

[3] Abhay Kochhar, Mary E. Galanko , Mazen Soliman, Hoda Abdelsalam, Luca Colombo , Yi-Chung Lin, Gabriel Vidal-Álvarez , Tamal Mukherjee, "Resonant Microelectromechanical Receiver," IEEE, 2019.

[4] Q. Gu, RF System design of transceivers for Wireless Communications, United States of America: Springer, 2005.

[5] J. O'Reilly, Telecommunications Principles, Van Nostrand Reinhold UK: Colset Private, 1984.

[6] C. Drentea, Modern Communications Receiver Design and Technology, Norwood: Artech House, 2010.

[7] M. S. John G. Proakis, Communication Systems Engineering, New Jersey: Prentice Hall, 2002.

[8] J. R. JAMES, Microstrip Antenna Theory and Design, London: Peter Peregrinus Ltd, 1981.

[9] D. R. B. Waterhouse, Microstrip Patch Antennas: A Designer's Guide, New York: Springer Science+Business Media, 2003.

[10] R. Garg, Microstrip Antenna Design Handbook, Norwood: ARTECH HOUSE INC., 2001.

[11] G. A. T. Warren L. Stutzman, Antenna Theory and Design, 3rd Edition, Danvers: John Wiley & Sons, Inc., 2013.

[12] G. Murillo, Integration for a resonant N/MEMS for energy harvesting from ambient vibrations PhD Thesis, Bellaterra: Universitat Autonoma de Barcelona, 2011.

[13] C. P. Vega, Sistemas de Telecomunicación, Cantabria: Servicio de Publicaciones de la Universidad de Cantabria, 2007.

[14] J. Chitode, Communication Theory, India: Technical Publications Pune, 2006.

[15] H. J. D. L. Santos, Introduction to Microelectromechanical Microwave Systems, Norwood: ARTECH HOUSE, 2004.

[16] T. A. Milligan, Modern Antenna Design, New Jersey: John Wiley & Sons, Inc., 2005.

[17] C. A. Balanis, ANTENNA THEORY ANALYSIS AND DESIGN, New Jersey: John Wiley & Sons, Inc., 2005.